SOVIET PHYSICS

USPEKHI

A Translation of Uspekhi Fizicheskikh Nauk

É. V. Shpol'skiĭ (Editor in Chief), S. G. Suvorov (Associate Editor),
D. I. Blokhintsev, V. I. Veksler, S. T. Konobeevskiĭ (Editorial Board).

SOVIET PHYSICS USPEKHI (Russian Vol. 83, Nos. 3 and 4) JANUARY-FEBRUARY, 1965

548.0:539.12.04

FOCUSING OF ATOMIC COLLISIONS IN CRYSTALS

R. I. GARBER and A. I. FEDORENKO

Usp. Fiz. Nauk 83, 385-432 (July, 1964)

1. INTRODUCTION

AT the present time, because of the rapid development of atomic energy, study of the effect of nuclear radiations on the structure and properties of solid materials is being carried on more intensively than ever before. The interest in this relatively new problem is due to the practical importance of the change in the mechanical and physical properties of materials used in construction of nuclear apparatus, primarily nuclear reactors.

Study of the nature of radiation damage in the crystal lattice also has great possibilities for the development of solid state physics.

In the theories developed in the 1950's for the formation of radiation damage in solid materials (the theories of cascade displacements of atoms [1-3], thermal spikes [4,5], displacement zones, and others), the regularities of the atomic arrangement in the crystal lattice have not been properly taken into account. The main premises of these theories are applicable both to crystalline and amorphous media, except perhaps the mechanisms of vacancy formation and implanting of interstitial atoms.

On bombardment of a crystal by charged or neutral particles, the influence of the regular location of the atoms in the lattice leads to preferential propagation of a wave of atomic collisions along the most closely packed directions. This phenomenon has been called the focusing of atomic collisions.

The first information on this type of focusing was obtained in 1954 by Wehner in studies of cathode sputtering [8]. At the present time the number of similar experimental investigations is approaching one hundred. Theoretical papers have also appeared [9-15]. High-speed electronic computers are used for solving some of the problems in this field [16].

The study of atomic collision focusing is very important not only for investigation of radiation damage, but also in connection with studies of cathode sputtering [17]. The sputtering of surfaces under the action of fast particles has acquired particular importance in connection with the flight of artificial Earth satellites and space ships, whose surfaces are subjected to bombardment by particles in the upper layers of the atmosphere and in interplanetary space [18]. The laws governing the destruction of metals by ionic bombardment are important also in design of plasma and ion engines for space ships [19]. Finally, study of the mechanism of metallic sputtering by ions of relatively high energy is very important since this process affects the contamination of plasmas in thermonuclear devices [20-21].

In this review we have systematized and, as far as possible, completely explained the theoretical treatments of the mechanism of atom focusing occurring in the crystal lattice when solid materials are bombarded by fast particles, and we have brought together the main experimental results.

2. THEORY OF RADIATION DAMAGE

2.1. Cascade Displacements of Atoms

In the passage of a high energy particle through a solid body, transfer of energy from the particle to the lattice can occur initially only by means of ionization, and the probability of a displacing collision is small. Seitz [22] established that at high energies the energy loss of a particle through Rutherford scattering by nuclei amounts to ~ 0.1%.

However, as the particle energy is decreased, the ionization loss falls rapidly and below a definite critical energy goes to zero. At the same time there is an

increased probability of a displacing collision in which a rather large amount of kinetic energy (from 10 to probably 10^5 eV) is transferred from the bombarding particle to one of the stationary atoms of the lattice.

The moving primary displaced atom, by colliding with other lattice atoms that are in equilibrium positions and transferring to them a certain threshold amount of energy (~ 25 eV), produces so called secondary displaced atoms and forms in its path a whole cascade of such displacements.

Thus, the theory of cascade displacements of atoms during irradiation suggests the appearance of Frenkel pair defects (a vacancy and an interstitial atom), the number of which we can calculate [22]. At a sufficiently high temperature the vacancies and interstitial atoms can diffuse in the lattice, and if they come sufficiently close together, recombination can occur. In addition, the vacancies and interstitial atoms can segregate, collecting in clusters. Present-day transmission electron microscope techniques [23-27] allow observation of such clusters in irradiated materials.

2.2. Thermal Spikes

According to Seitz [22], only a small fraction of the energy of a primary knock-on atom is expended in formation of Frenkel defects. The remaining part of the energy of the displaced atom, when its mean free path becomes commensurate with the interatomic distance, will be transferred to neighboring atoms. As a result there occurs a rapid heating of a limited region with a diameter of about 40 interatomic distances, containing ~ 60,000 atoms.

The temperature of this region rises to approximately 4000 degrees, and during this thermal spike (of duration 10^{-12} sec) the material acts essentially like a liquid and not a solid material. Kosevich and Tanatarov showed [29] that in the process of solidification of the melt in the region of a thermal spike, very great negative pressure can arise in the liquid, producing under certain conditions a rupture in the liquid. The latter phenomenon can lead to formation of cavities in the material after complete solidification. Proofs of the existence of local melting during irradiation were obtained by Gonser and others [30-32], who observed small regions of the liquid phase in crystals of GaSb bombarded by deuterons and Ge bombarded by neutrons.

Since the specific volume of the liquid phase in the region of the melting is greater than the specific volume of the surrounding solid phase, this leads to plastic deformations around the region of local melting. As the result, in the region of greatest mechanical stress, at a distance of not more than 10 Å from the center of the spike, dislocations should be formed [4]. Since the dislocation lines can be either closed, or interrupted at the crystal surface, these dislocations form in the crystal individual loops or systems of loops. Recently these loops and systems of loops have been observed with an electron microscope in a number of irradiated metals [33,34].

2.3. Displacement Zones

If the excitation of the atoms of the material by the energy transferred to them by primary knock-on atoms is sufficiently great that rupture of the bonds begins to occur, then, according to the mechanism proposed by Brinkman [6], they begin to be displaced from their equilibrium positions in the lattice, and are implanted in interstitial positions. As a result there is formed a region of broken-up material which, for a period of 1.2×10^{-12} sec [35], may be in a gaseous or liquid state, after which it solidifies. In the course of this disturbance, recrystallization can occur with a mixing of all the atoms located in this region and the formation of a small number of microcrystals with completely new orientations. Thus, all the atoms will be displaced from the positions which they previously occupied and will occupy new positions, forming a so-called displacement zone.

This process must be distinguished from the thermal spike described above. According to Brinkman [6], Frenkel pair defects produced by irradiation cannot be preserved in displacement zones. Furthermore, the recrystallization of the entire volume of the displacement zone should result in sharply defined boundaries which are not present in the case of thermal spikes.

The dimensions of a displacement zone can be approximately established from the difference between the energy of the primary knock-on atom at the beginning of the displacement zone formation and the mean energy of an atom in the zone of melting. Calculation [6] has shown that for copper the displacement zones produced by irradiation with 2 MeV neutrons consist of 2×10^4 atoms and have, for the case of spherical shape, a diameter of ~ 75 Å.

The existence of displacement zones is somewhat problematical and probably has a significance only for heavy metals. The theory of the formation of displacement zones is incomplete and requires further development.

Each of the theories enumerated above has its weaknesses. Attempts to introduce specific corrections have not as yet been successful. In all of these theories it has been assumed that the atoms in the solid material are distributed statistically; that is, any influence of the regular position of the atoms in the crystal lattice on the distribution of the collisions has been completely neglected. Therefore it should not surprise us to find discrepancies between the theoretical predictions and the experimental data. Actually the mechanism of the collision of particles in the crystal lattice of a solid material is much more

complicated than was assumed by the early theories of radiation damage.

2.4. Replacement Collisions

In some collisions the bombarding atom, having knocked a stationary atom from its lattice site, cannot move away from the vacancy which it has formed, since its residual energy is insufficient. Recombining with the vacancy, it diffuses its kinetic energy in the form of thermal oscillations of the lattice. Collisions of this type, which lead to a change in the type of atom located in certain lattice sites, are called replacement collisions.

The mechanism of replacement collisions proposed by Kinchin and Pease[36] is extremely important in discussion of radiation effects in alloys. In particular, with this mechanism it has been possible to explain satisfactorily the disordering process which occurs upon irradiation of the ordered alloy $MnNi_3$[37].

2.5. Crowdions

If an atomic collision leading to replacement occurs in one of the close-packed directions, for example ⟨100⟩, in a face-centered cubic crystal, the implanted atom will be confined inside a unit cell and its residual energy will be distributed among the neighbors. One of its six nearest neighbors can be ejected into the center of a neighboring unit cell. If this happens, then the newly implanted atom will have its kinetic energy "channeled" in the ⟨100⟩ direction. Huntington[38] has shown that the energy associated with this process is almost independent of the position of the implanted atom along the ⟨100⟩ direction.

Implanted atoms, located in a close-packed row and shifting the array of atoms for several interatomic distances along this row, form a crowding of the atoms, in which P + 1 atoms occupy P places along the close-packed row. Such crowdings have received the name crowdions[39]. Lomer and Cottrell[40] showed that crowdions exist in copper, traveling along the ⟨100⟩ direction for many interatomic distances.

2.6. Depleted Zones

Seeger[41,42] showed that in face-centered cubic metals, at the end of the range of a primary displaced atom, a zone is formed in which an appreciable fraction of the atoms are displaced. However, in contrast to Brinkman's displacement zone, a fraction of the displaced atoms do not remain near the multiple vacancy produced and do not return to it as assumed by Cottrell[43], but leave this zone by a distance of the order hundreds of Å, migrating as dynamic crowdions. In this way there is formed a so-called depleted zone of diameter ~ 10 Å with a reduced density, in which 20–30% of the atoms are missing (Fig. 1).

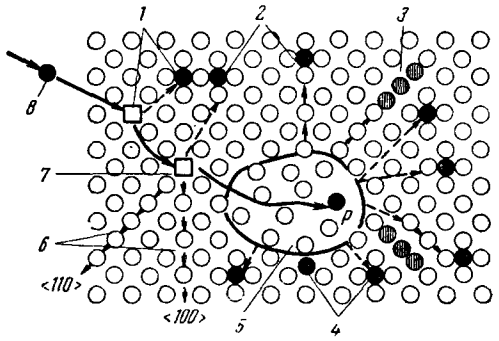

FIG. 1. Schematic representation of radiation damage produced by a fast neutron in copper. 1 – Close Frenkel pair; 2 – exchange or replacement collisions; 3 – dynamically migrating crowdion; 4 – interstitial atoms; 5 – depleted zone; 6 – focusons; 7 – vacancy; 8 – primary knock-on atom.

Irradiated materials can be strengthened by the existence of such zones, since they will hinder the movement of dislocations. Seeger's assumptions are in agreement with the experimental data obtained for copper.

Such forms of radiation damage as replacement collisions, crowdions, and depleted zones were observed after the crystal structure of the irradiated materials began to be taken into account properly in the discussion of radiation damage mechanisms. The role of the crystal lattice is also important in the formation of such types of radiation damage as focusons.

Crowdion collisions represent a means of transporting a concentration of atoms over significant distances. The focusing of atomic collisions is a mechanism which permits the transport, along a linear chain of atoms in a close-packed direction, of impact energy received by one of the atoms in the chain. Let us discuss what this mechanism of radiation damage is, what experimental confirmations exist for it, and how with its aid we can explain the effect of irradiation on the properties of solid materials.

3. FOCUSING OF ATOMIC COLLISIONS

3.1. Propagation of Collisions Along a Linear Chain of Atoms

Silsbee[9] in 1957 was the first to point out that in a close-packed isolated chain of equally spaced atoms, focusing of an impact can occur under certain conditions.

It was assumed that the atoms interact with two-body repulsive central forces of the Born-Mayer type:

$$V(r) = A \exp\left(-\frac{r}{a}\right). \qquad (1)$$

Over a wide range of energies of the moving particle (for heavy atoms up to several tens of keV) the interaction between the moving and stationary atoms can be calculated to a first approximation by use of the elastic-hard-sphere model. In this model the potential

(1) is replaced by the interaction potential of two hard spheres:

$$V(r)=\frac{1}{2}E_0, \tag{2}$$

where E_0 is the kinetic energy of the moving atom.

From (1) and (2) we obtain the following expression for the diameter of the hard sphere:

$$r=a\ln\frac{2A}{E_0}. \tag{3}$$

For the particular case of irradiation of copper, Huntington[38] found that the best approximation was given by the potential

$$V(r)=0.038\exp\left[-\frac{17.2(r-D)}{D}\right]\text{ eV}, \tag{4}$$

where D is the distance to the nearest neighbor atom, which is in its equilibrium state.

The effective hard-sphere diameters calculated from (3) and (4) for copper, for various ion energies E, are listed in Table I[44], where the value of D has been taken to be the smallest distance between copper atoms in the ⟨110⟩ direction, 2.55×10^{-8} cm.

Table I

E, eV	11.6	50	100	400
r, Å	2.23	1.57	1.51	1.28
D/r	1.41	1.80	1.69	1.99

Silsbee's analysis shows that, for values of r close to D and for small values of D (i.e., $D/r=\alpha<2$); the moving particle transfers its momentum to the stationary atoms of the close-packed chain in such a way that the momentum is propagated along the chain at an angle θ to its axis, which is less at each successive collision. The angle θ (see Fig. 2) is determined by the following equation:

$$\sin\theta_n=\sin\theta_{n-1}[\alpha\cos\theta_{n-1}-(1-\alpha^2\sin^2\theta_{n-1})^{1/2}]. \tag{5}$$

The energy transferred in a series of successive collisions is given by

$$E_n=E_{n-1}(1-\alpha^2\sin^2\theta_{n-1}). \tag{6}$$

Since the angle θ becomes steadily smaller with each successive collision, for sufficiently small values of θ Eq. (5) reduces to

$$\theta_n=\theta_{n-1}(\alpha-1). \tag{7}$$

The ratio θ_n/θ_{n-1}, which indicates the degree of focusing, has been called the focusing parameter Λ:

$$\Lambda=\theta_n/\theta_{n-1}. \tag{8}$$

For small angles we obtain from equation (7)

$$\Lambda=\alpha-1. \tag{9}$$

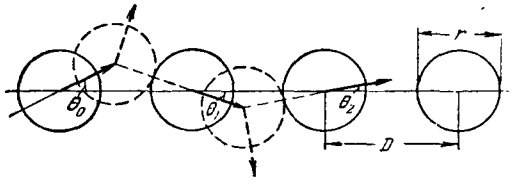

FIG. 2. Focusing effect in the propagation of an impact along a linear chain of hard spheres.

3.2. Focusing and Crowdion Collisions

Two different types of collisions can take place, depending on whether the parameter Λ is greater or less than unity[10].

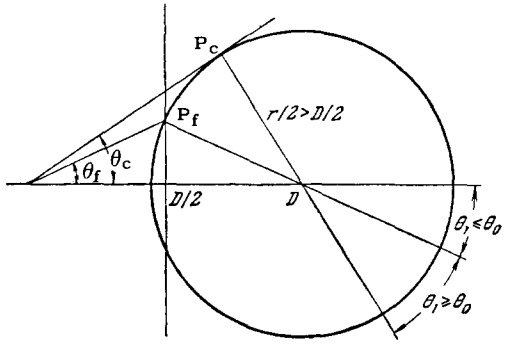

FIG. 3. Focusing and crowdion collisions.

a) Λ < 1 (cos $\theta_0 > \alpha/2$; the collision point is P_f in Fig. 3, to the left of D/2). Here the conditions are realized for focusing collisions, which result in the transfer of impact energy only along the chain of atoms. Sequences of such focusing collisions have received the name focusons. Under certain limiting conditions the focuson begins to be propagated in the form of consecutive binary central collisions with zero angle (Fig. 4). The limiting energy below which a focuson begins to be propagated along the axis of the chain with essentially no loss of energy is known as the focusing energy E_f.

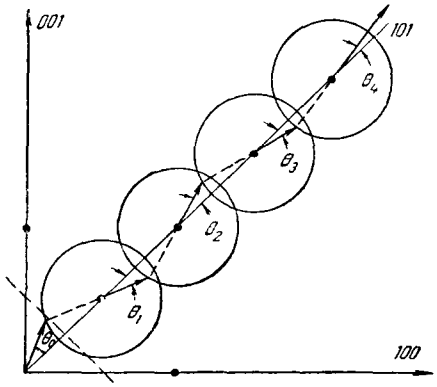

FIG. 4. Focusing collisions along the <101> direction in a face-centered cubic metal.

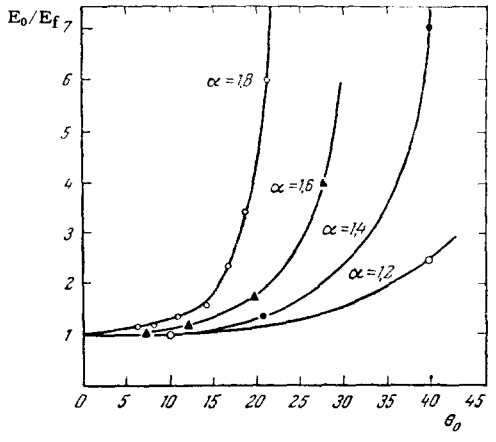

FIG. 5. Ratio of the incident particle energy E_0 to the energy E_f transmitted along a chain of atoms for different values of θ_0 and α.

Figure 5 shows the ratio of the energy of the incident particle E_0 to the energy E_f which is transferred along the chain of atoms, for different values of θ_0 and α[9]. For $\alpha = 1.6$ and $\theta_0 = 25°$, 36% of the initial energy E_0 will be transferred by the focuson.

From the focusing condition $\alpha = D/r < 2$, it can be seen that the focusing effect occurs preferentially along close-packed rows of atoms. Such rows are formed by atoms located along the ⟨100⟩ direction in the case of a simple cubic lattice, the ⟨110⟩ direction in a face-centered cubic lattice, and the ⟨111⟩ direction in a body-centered cubic lattice.

For the propagation of a focuson in copper along the ⟨110⟩ direction, using the potential of Eq. (4) with the constants $A = 2.1 \times 10^4$ eV and $a = D/13$[38], we obtain

$$E_f = 2A \exp(-6.5) = 63 \text{ eV}. \quad (10)$$

For this value of the energy E_f the relative loss of energy in the close-packed ⟨110⟩ direction, ϵ^{110}, amounts to 1.1% [see Eq. (12)].

Focusons can be propagated large distances from their place of origin and can produce there displacement effects leading in different cases either to production of radiation damage or to ejection of the last atom of the chain from the crystal (i.e., sputtering).

b) $\Lambda > 1$ ($\cos\theta_0 < \alpha/2$; the collision point in Fig. 3 is P_c, to the right of D/2). Collisions occurring under these conditions have been named by Leibfried[10] crowdion collisions. In this case (Fig. 6) there is a high probability for the formation of a vacancy and a compression of the atoms, similar to the crowdions suggested by Paneth[39]. If the initial angle θ_0 is not very large, then although a defocusing of the collisions occurs as a result of the condition $\Lambda > 1$, the crowdion is propagated along the chain for a large distance.

The maximum angle θ_c for which formation of focusons and crowdions will occur, as can be seen from Fig. 3, is given by the condition

$$\cos\theta_c = \frac{1}{\alpha}. \quad (11)$$

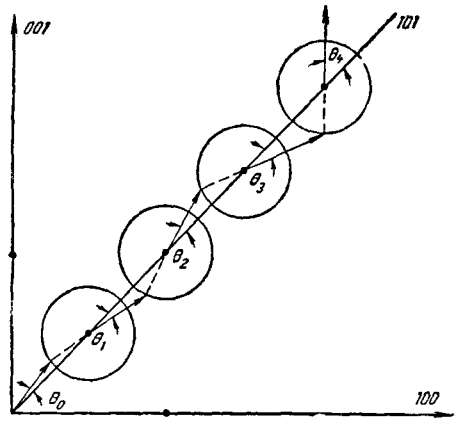

FIG. 6. Crowdion collisions along the <101> direction in a face-centered cubic metal.

The distinction between a crowdion and a focuson lies in the fact that a crowdion transfers not only energy (momentum) like a focuson, but also matter. According to Seeger[42], crowdion collisions play an important role in the formation of the depleted zones discussed above.

4. FORMATION OF FOCUSONS IN FACE-CENTERED CUBIC METALS

4.1. Focusing of Atomic Collisions in the ⟨110⟩ Direction

Silsbee[9] and Leibfried[10] have shown that during the propagation of focusons along the close-packed ⟨110⟩ direction in face-centered cubic metals it is impossible to neglect completely the effect of neighboring atoms. But, since the hard-sphere potential falls off very rapidly with distance, it is quite sufficient to consider the effect on focuson propagation along the ⟨110⟩ direction of the ring of the closest four atoms 011, $0\bar{1}1$, $1\bar{1}0$ and 110, located in the two neighboring {100} planes (Fig. 7a).

Calculation of the fractional energy loss in the interaction with these four atoms leads to the following expression[10]:

$$\varepsilon^{110} = \frac{\Delta E}{E_f} = 2\left[\exp\left(-\frac{3D}{8a}\right) - \exp\left(-\frac{D}{2a}\right)\right], \quad (12)$$

where ΔE is the energy loss in a collision. The number of focusing collisions in this case will be $n_\epsilon = 1/\epsilon$, and the range of the focuson along the ⟨110⟩ direction will be $R_f = n_\epsilon D$.

For copper Leibfried[11], using the potential of Eq. (4) with the constants $A = 2.1 \times 10^4$ eV, $a = D/13$[38], and $E_f = 63$ eV, obtained $\epsilon^{110} = 1.1 \times 10^{-2}$, and the maximum focuson range corresponding to these values of E_f and ϵ^{110} was found to be $R_f = 90D$.

Nelson and Thompson[45] calculated the range of focusons in gold in the ⟨110⟩ direction for different values of E_f and D/a (Table II). For D/a = 15 and $E_f = 800$ eV, they found ϵ^{110} for gold to be 5×10^{-3}.

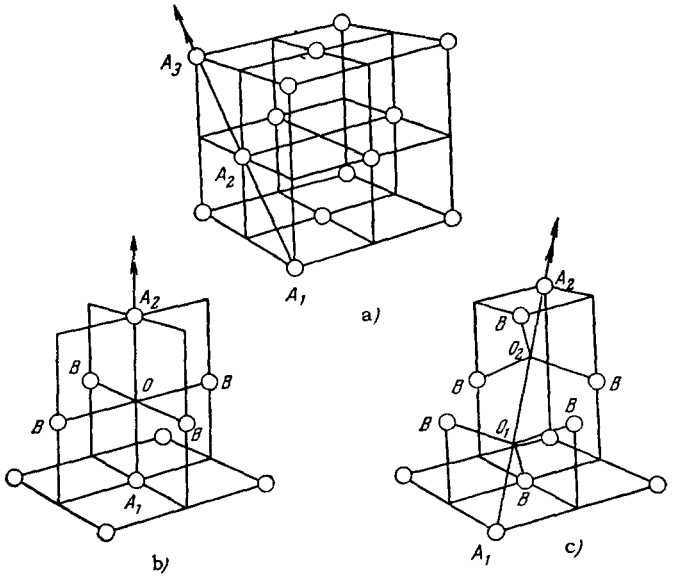

FIG. 7. a) Focusing of atomic collisions in the <110> direction; b-c) replacement with focusing in the <100> and <111> directions, respectively.

Their calculation used the potential of Eq. (1) with the constant $A = 0.8 \times 10^6$ eV. The use of this potential is justified by the fact that the value of compressibility obtained from it without considering the effect of free electrons is 0.33×10^{-12} cm^2 dyne^{-1}, which is in very good agreement with the experimental value 0.54×10^{-12} cm^2 dyne^{-1}.

According to Silsbee, focusing in the ⟨100⟩ direction in a face-centered cubic metal is impossible, since an atom displaced in the ⟨100⟩ direction must collide with an atom in a ⟨110⟩ row before it approaches an atom in the ⟨100⟩ row. However, with a more rigorous calculation, we can explain also the experimentally observed focusing in the ⟨100⟩ and ⟨111⟩ directions.

Table II

E_f, eV	320	640	960	1250	1600
R_f, Å	190	300	400	500	600
D/a	13.2	14.6	15.4	16.0	16.4

4.2. Replacement with Focusing in the ⟨100⟩ Direction

Let us consider an atom A_1 moving in the ⟨100⟩ direction through a ring of four B atoms and colliding with the atom A_2 (Fig. 7b). The result of the deflection φ of the atom A_1 during its passage through the ring of B atoms (Fig. 8a) will be a small deviation of its trajectory angle θ_1. This deflection depends on the energy of the atom A_1. Nelson and Thompson [45], discussing this problem, found that

$$\varphi = \frac{2}{3}\theta_1 \frac{Aa^2}{ED^2} \exp\left(-\frac{3D}{4a}\right). \quad (13)$$

This expression can be extended to any plane of incidence, and therefore, since φ is proportional to θ_1, the ring of B atoms acts like a condensing lens with a focal length $f = (D/\sqrt{2})\,(\theta_1/\varphi)$, i.e.,

$$f^{100} = \frac{3}{2\sqrt{2}} \frac{E}{A} \frac{a^2}{D} \exp\left(\frac{3D}{4a}\right). \quad (14)$$

The condition for focusing of the collision of atoms A_1 and A_2 is $\theta_1 > \theta_2$ (Fig. 8a). Here $D\sqrt{2} > 4f^{100}$. Hence the maximum energy for formation of a focuson in the ⟨100⟩ direction, Ef^{100} will be, according to Nelson and Thompson [45],

$$E_f^{100} = \frac{A}{3} \frac{D^2}{a^2} \exp\left(-\frac{3D}{4a}\right), \quad (15)$$

and the ratio of the maximum energies for the formation of focusons in the ⟨100⟩ and ⟨110⟩ directions is

$$\frac{E_f^{100}}{E_f^{110}} = \frac{1}{6} \frac{D^2}{a^2} \exp\left(-\frac{D}{4a}\right). \quad (16)$$

The fractional energy loss of the atom A_1 on passing through the ring of B atoms will be

$$\varepsilon^{100} = \frac{1}{E^2} \frac{D^2A^2}{a^2} \exp\left(-\frac{3D}{2a}\right), \quad (17)$$

and when $E = Ef^{100}$,

$$\varepsilon_f^{100} = 9\frac{a^2}{D^2}. \quad (17a)$$

If we neglect the weakening effect of the B atoms at the time of the collision, the minimum energy Ef^{100} for collision of atoms in a ⟨100⟩ direction can be obtained by equating the kinetic energy of the atom A_1 to the difference in potential energy between the points A_1 and 0 in Fig. 8a, i.e.,

$$E_f^{100} = 5A \exp\left(-\frac{D}{a\sqrt{2}}\right) \quad (18)$$

or, referred to E_f^{100},

$$\frac{E_i^{100}}{E_f^{100}} = \frac{5}{2} \exp\left(-\frac{D}{a} \frac{\sqrt{2}-1}{2}\right). \quad (18a)$$

The condition for replacement of A_1 atoms by A_2

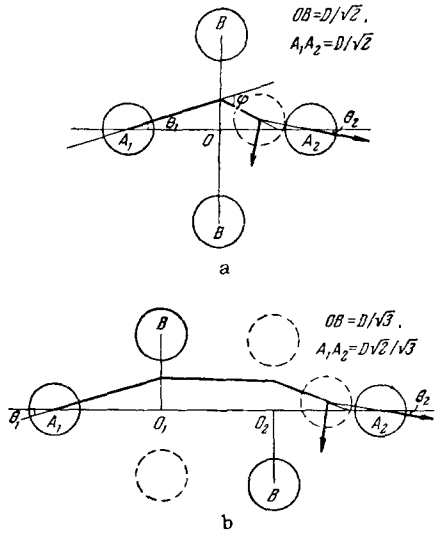

FIG. 8. Focusing effect in a) <100> and b) <111> directions.

atoms is that the A_1 atom after collision with the A_2 atom should again pass the point 0, i.e.,

$$R \leqslant \frac{D}{\sqrt{2}}.$$

In the limit this condition is identical with the limiting conditions for formation of focusons in the ⟨110⟩ direction and is fulfilled for certain values of θ_1 at an energy A exp $(-D/a\sqrt{2})$. This energy is naturally less than E_1^{100}, the energy required for penetration of the ring, and therefore all collisions in the ⟨100⟩ direction eventually lead to replacements, and when the energy becomes less than E_f^{100}, focusons are formed.

This process in collisions of atoms along a row was called by Nelson and Thompson [45] replacement with focusing. The idea of replacement collisions was first introduced, as we have mentioned above, by Kinchin and Pease [36]. However they did not suggest any concrete mechanism for explaining these collisions.

Since the energy losses are accurately known only for $\epsilon^{100} < 0.2$, there is no necessity of obtaining an exact expression for the number of replacements n_r^{100} in the focusons formed at an energy E_f^{100}. As a very rough evaluation we can take

$$L_r^{100} \approx \frac{1}{2}\varepsilon_f^{100},$$

or

$$L_r^{100} \approx \frac{D^2}{20a^2}. \qquad (19)$$

4.3. Replacement With Focusing in the ⟨111⟩ Direction [45]

From Fig. 7c it is evident that the atom A_1, having received an impact in the ⟨111⟩ direction, is focused on passing through two rings of three B atoms and, colliding with the atom A, replaces it. At high energies the atom A_1 loses practically no energy, and therefore both rings of B atoms will have the same focal length (Fig. 8b),

$$f^{111} = \frac{19}{3}\frac{E}{A}\frac{a^2}{D}\exp\left(-\frac{D}{2a}\sqrt{\frac{19}{12}}\right). \qquad (20)$$

The limiting energy E_f^{100} for which $\theta_1 > \theta_2$ and focusing is observed is

$$E_f^{111} = \sqrt{\frac{6}{19}}\frac{AD^2}{a^2}\exp\left(-\frac{D}{2a}\sqrt{\frac{19}{12}}\right), \qquad (21)$$

and

$$\frac{E_f^{111}}{E_f^{110}} = \frac{1}{2}\sqrt{\frac{6}{19}}\frac{D^2}{a^2}\exp\left[-\frac{D}{20}\left(\sqrt{\frac{19}{21}}-1\right)\right]. \qquad (22)$$

The minimum energy required for passage through one ring is

$$E_1^{111} = 4A\exp\left(-\frac{D}{a\sqrt{3}}\right), \qquad (23)$$

and

$$\frac{E_1^{111}}{E_f^{111}} = 2\exp\left(-\frac{D}{2a}\frac{2-\sqrt{3}}{\sqrt{3}}\right). \qquad (23a)$$

The fractional energy loss per replacement is

$$\varepsilon^{111} = \frac{3}{2}\frac{1}{E^2}\frac{D^2A^2}{a^2}\exp\left(-\frac{3D}{2a}\right), \qquad (24)$$

and, for $E = E_f^{111}$,

$$\varepsilon_f^{111} = \frac{19}{4}\frac{D^2}{a^2}. \qquad (24a)$$

The number of replacements n_r^{111} occurring in the propagation of focusons starting with energy E_f^{111} (calculated with an accuracy of 5%) for energy losses $\epsilon_f^{111} < 0.2$ (for $a \approx D/5$), will be, according to a rough evaluation,

$$n_r^{111} \approx \frac{D^2}{10a^2}. \qquad (25)$$

Table III lists values of E_f, E_1, ϵ_f, and n_f in the ⟨110⟩, ⟨100⟩, and ⟨111⟩ directions for copper and gold. For copper the potential of Leibfried [10] was used, and for gold the potential of Nelson and Thompson [45]. The

Table III

Crystallographic direction	E_f, eV		E_1, eV	
	Cu	Au	Cu	Au
⟨110⟩	60	800	1	1
⟨100⟩	65	700	10	90
⟨111⟩	490	7300	44	500

Crystallographic direction	ε_f		n_f	
	Cu	Au	Cu	Au
⟨110⟩	0.011	0.006	90	170
⟨100⟩	0.053	0.040	9	13
⟨111⟩	0.027	0.021	17	45

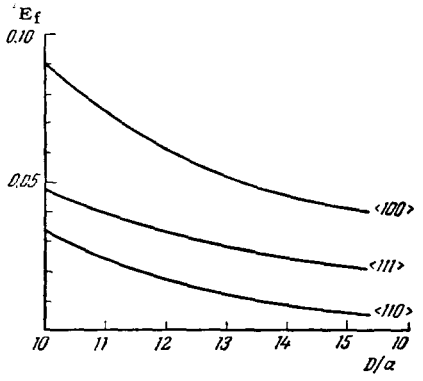

FIG. 9. Energy loss as a function of D/a.

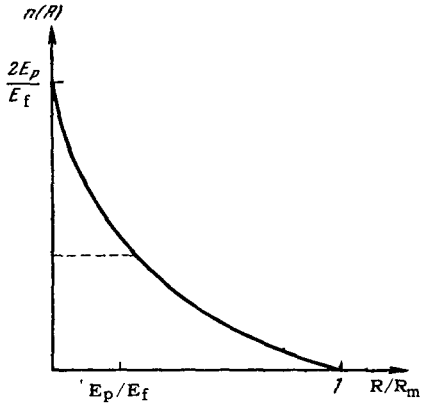

FIG. 10. Number of focusons n(R) with range greater than R. The dashed line gives n(R) for the case where focusons with initial energy less than E_f are neglected.

ratio of the fractional energy loss in the ⟨100⟩ and ⟨111⟩ directions to ϵ_f^{110} is shown as a function of D/a in Fig. 9.

4.4. Dependence of the Number of Focusons on the Total Number of Displacements

Leibfried[11] calculated the number of focusons ν_f formed in bombardment of a crystal as a function of the total number of atomic displacements ν:

$$\nu_f = 1.5\nu\left\{1-\frac{n^*}{n^*(0)}\left[1+\ln\frac{n^*(0)}{n^*}\right]\right\}. \qquad (26)$$

Here n^* is the average number of atomic collisions, and $n^*(0)$ is the number of atomic collisions beginning from a state of rest.

Since $n^*(0) \approx 10^2$, for $n^* = 50 = n^*(0)/2$, the number of focusons formed is $\nu_f(E, 50) \cong 0.22\nu$. This value is five times larger than the number of crowdions formed under the same conditions: $\nu_c(E, 50) \cong \nu \times 10/n^{*2} = 4 \times 10^{-3}\nu$.

The number of focusons in the energy interval dE, produced by a primary displaced atom with an energy $E_p \geq E_f$, is equal to[11]

$$\nu(E_f, E) = \frac{2E_p}{E_f^2}\frac{12a}{D}\ln\frac{E_f}{E} \text{ with } E \ll E_f; \qquad (27)$$

here E_f is the energy limit for formation of a focuson, and E is the energy of the focuson. Since a/D = 1/13, (27) ultimately acquires the form

$$\nu(E_f, E) = \frac{2E_p}{E_f^2}\ln\left(\frac{E_f}{E}\right). \qquad (28)$$

Correspondingly, it is possible to determine the number of focusons with a range in the interval dR:

$$\nu(E_f, R) = \frac{2E_p}{E_f^2}\ln\left(\frac{R_m}{R}\right); \qquad (29)$$

here R is the focuson range and R_m is the maximum range. From (29) we can obtain the number of focusons $n(E_p, R)$ with a range greater than R (Fig. 10):

$$n(E_p, R) = \int_R^{R_M}\nu(E_f, R')\,dR' = \frac{2E_p}{E_f}\left\{1-\frac{R}{R_m}\left(1+\ln\frac{R_m}{R}\right)\right\}. \qquad (30)$$

4.5. Interaction of Focusons With Lattice Defects[11]

In irradiation of a face-centered cubic metal, as the result of formation of focusons along a close-packed direction, displacement of a chain of several atoms can occur in the direction of the impact. Here each atom will occupy the site of the preceding atom. On encountering a lattice packing defect of the split dislocation type, the focuson should form a Frenkel defect. Leibfried[11] calculated the number of Frenkel defects arising in this case:

$$\nu_D = \frac{2E_p}{E_f}\frac{aR_m}{10\lambda^2}. \qquad (31)$$

Here a is the splitting separation of the dislocation and λ is the average distance between dislocations in the lattice. The number of Frenkel defects formed by a focuson on meeting a dislocation will be proportional to the density of dislocations $\rho_D = 1/\lambda^2$. However, this proportionality extends only up to the density at which the dislocations begin to overlap each other. The maximum number of Frenkel defects formed, which is reached at a very high dislocation density, is of course equal to the total number of focusons ν_f. The maximum value of the coefficient $aR_m/10\lambda^2$ cannot exceed 1/3, the value at which the number of Frenkel defects produced becomes constant and independent of the dislocation density (Fig. 11).

Using the cascade model of radiation damage

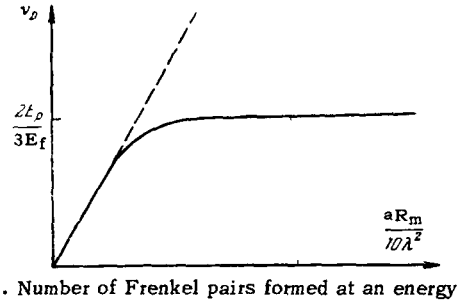

FIG. 11. Number of Frenkel pairs formed at an energy E_p, as a function of the dislocation density $1/\lambda^2$.

formation, according to which the number of Frenkel defects formed by a primary displaced atom with energy E_p is equal to

$$\nu(E_p)=\frac{E_p}{2E_d} \quad (E_p \gg 2E_d),$$

where E_d is the limiting energy of displacement, and taking account of dislocations, Leibfried calculated the total number of Frenkel pairs arising in irradiation, due to intersection of focusons with dislocations,

$$\nu_t(E_p)=\nu(E_p)+\nu_D(E_p)=\nu(E_p)\left(1+\frac{4E_d}{E_f}\frac{aR_m}{10\lambda^2}\right). \quad (32)$$

For copper, using E_f = 63 eV and E = 22 eV, he obtained

$$\nu_t=\nu(E_p)\left(1+1.4\frac{aR_m}{10\lambda^2}\right). \quad (33)$$

5. FORMATION OF FOCUSONS IN BODY-CENTERED CUBIC METALS

5.1. Focusing of Atomic Collisions in the ⟨111⟩ Direction

The interaction between the atoms in body-centered cubic lattices can be described by the repulsive potential of (1). However the constants A and a used in the case of face-centered metals such as Cu, Ag, and Au are not very suitable for other metals. Therefore Brinkman[46] suggested an empirical expression for the atomic interaction potential for several metals with Z > 25. Nelson and Farmery[47] used Brinkman's potential for evaluating the focusing conditions in body-centered cubic metals. If we take D ≈ a_0, where a_0 is the lattice constant, then Brinkman's potential acquires the form of (1) with the constants

$$A=1.9\cdot10^{-6}E_RZ^{1/2} \text{ and } a=\frac{1.5a_B}{Z^{1/3}},$$

where Z is the atomic number, E_R is the Rydberg energy, and a_B is the Bohr radius for hydrogen. Brinkman used this form of potential for calculating the elastic constants for various metals and obtained relatively satisfactory agreement with measured values. The parameter a for the majority of body-centered cubic metals is assumed to lie somewhere between D/10 and D/20. For tungsten, for example, the Born-Mayer constants will be A = 4.9 × 10^5 eV and a = D/17.[47]

In body-centered cubic structures the densest packing of atoms occurs in the ⟨111⟩ direction, and we expect the greatest probability for formation and propagation of focusons to occur along this direction. In the hard-sphere approximation the focusing condition in this case according to Silsbee[9] will be $D^{111}/r \leq 2$, where D^{111} is the distance of separation between nearest neighbor atoms along the ⟨111⟩ direction. Since the diameter of the hard sphere depends on energy according to Eq. (2), the maximum energy E_f^{111} at which focusing will occur in the ⟨111⟩ direction can be found for the condition that $r = D^{111}/2$, where $D^{111} = 3a_0/2$.

Consequently,

$$E_f^{111}=A\exp\left(-\frac{\sqrt{3}}{4}\frac{a_0}{a}\right). \quad (34)$$

For face-centered lattices it has been shown that atoms located in neighboring rows affect the propagation of focusons. By a similar calculation we can determine the fractional energy loss per collision in propagation of a focuson in a body-centered lattice, taking into account nearest neighbor atoms:

$$\varepsilon_f^{111}=3\left[\exp\left(-0.38\frac{a_0}{a}\right)-\frac{1}{2}\exp\left(-0.43\frac{a_0}{a}\right)\right]. \quad (35)$$

Assuming a constant loss per collision, which is approximately valid as a result of the slow variation of diameter with energy, we can determine the number of collisions in a focuson beginning with E_f^{111}:

$$n_f^{111}=\frac{1}{\varepsilon_f^{111}}. \quad (36)$$

5.2. Focusing of Atomic Collisions in the ⟨100⟩ Direction[47]

The focusing energy in the ⟨100⟩ direction, obtained from the focusing condition, is

$$E_f^{100}=A\exp\left(-\frac{1}{2}\frac{a_0}{a}\right). \quad (37)$$

However, in this case the ring of neighboring atoms surrounding the ⟨100⟩ direction will affect the propagation of focusons along this direction. Figure 12

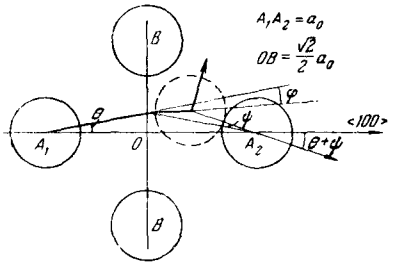

FIG. 12. Focusing effect in the <100> direction in a body-centered cubic metal.

shows how an atom A_1 moving with energy greater than E_f^{100} at a small angle θ to the ⟨100⟩ direction undergoes a deflection φ in passing through the ring of B atoms before its impact with the next atom in the ⟨100⟩ direction, A_2. Thus the ring of B atoms plays here, as in a face-centered lattice, the role of a lens with a focal length $f^{100} = a_0/2\ (\theta/\varphi)$ or, using the approximation of grazing collisions,

$$f^{100}=\frac{9}{8}\frac{E}{A}\frac{a^2}{a_0}\exp\left(\frac{3}{4}\frac{a_0}{a}\right). \quad (38)$$

From Fig. 12 in the approximation of small angles we can obtain

$$r\psi=\left(\frac{a_0}{a}-r\right)(2\theta-\varphi) \quad \text{for} \quad r<\frac{a_0}{2}, \quad (39)$$

where

$$\frac{\psi}{\theta}=\left(\frac{a_0}{2r}-1\right)\left(2-\frac{\varphi}{\theta}\right).$$

Thus,

$$\frac{\psi}{\theta}=\left(\frac{a_0}{2r}-1\right)\left(2-\frac{a_0}{2f^{100}}\right). \tag{40}$$

Figure 13 shows ψ/θ as a function of E for $a_0/a = 10$ with a correction introduced for the short interval in which grazing collisions are observed at low energies.

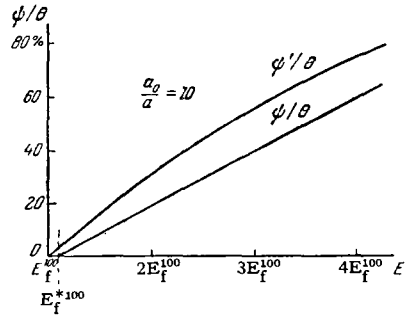

FIG. 13. Relative increase in angle between sequences of <100> collisions at energies above E_f^{100}.

For comparison we have shown in the plot of ψ/θ the relative increase in angle which occurs if we neglect focusing by the ring of B atoms. From these curves we can draw the conclusion that the ring changes the focusing condition to some extent, since the focusing energy E_f^{*100} increases somewhat and focusons are formed which then are defocused relatively slowly at energies greater than E_f^{100}. Therefore collision focusing which was initiated at $2E_f^{100}$ or even at $3E_f^{100}$ will be continued at a rather large distance before the energy E_f^{100} is reached, below which focusons will be propagated in the focused state.

Since the potential reaches a maximum value in the focusing ring, sequences of collisions involving penetration past the point O (Fig. 12) are replacement collisions. Sequences of collisions falling short of the point O accomplish only momentum transfer. In the hard-sphere approximation the latter will occur at E_f^{100}.

The fractional energy loss of a focuson in the ⟨100⟩ direction is

$$\varepsilon_f^{100}=2\left[\exp\left(-0.207\frac{a_0}{a}\right)-2\exp\left(-0.367\frac{a_0}{a}\right)\right]. \tag{41}$$

Assuming the energy loss per collision to be constant, we obtain the total number of collisions in a focuson beginning with E_f^{100}:

$$n_f^{100}=\frac{1}{\varepsilon_f^{100}}. \tag{42}$$

5.3. Focusing of Collisions in the ⟨110⟩ Direction[47]

From the discussion of the body-centered cubic structure it becomes clear that the focusing of atomic collisions in the ⟨110⟩ direction is due to the influence of a succession of rhombic-shaped rings of atoms surrounding this direction. The potential distribution of these rings is rather asymmetrical and forms the equivalent of a strongly astigmatic lens. The trajectories of atoms passing through these rings are shown in Fig. 14. A focuson propagated through a series of such rings will tend to be reflected from the X-atoms, which leads to oscillations of the successive collisions from side to side in the {100} plane.

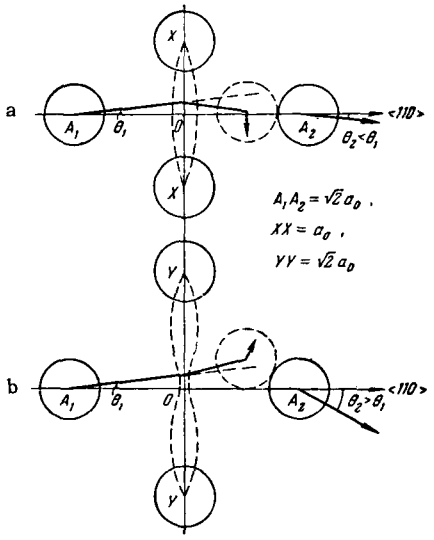

FIG. 14. Focusing effect in the <110> direction, showing astigmatism of the focusing "lenses."

True focusing, as we can see from Fig. 14a, occurs only for deflections in the {100} plane, that is, along the direction to the X-atoms. Proceeding from this we can evaluate the focusing energy of a series of collisions in the ⟨110⟩ direction. For this purpose let us consider the section X-X of the "lens." The focal length in this case will be

$$f_X^{110}=\frac{5}{4}\frac{a^2}{a_0}\frac{E}{A}\exp\left(\frac{\sqrt{5}}{4}\frac{a_0}{a}\right). \tag{43}$$

The focusing energy will then be

$$E_{f\,X}^{110}=\frac{\sqrt{2}}{5}\left(\frac{a_0}{a}\right)^2 A\exp\left(-\frac{\sqrt{5}}{4}\frac{a_0}{a}\right), \tag{44}$$

and the fractional energy loss is given by

$$\varepsilon_{f,X}^{110}=5\left(\frac{a}{a_0}\right)^2. \tag{45}$$

If there were no defocusing in the plane of the Y-Y section (Fig. 14b), then the number of collisions in the focuson would be

$$n_{f,X}^{110}=\frac{1}{10}\left(\frac{a_0}{a}\right)^2. \tag{46}$$

However, because of the astigmatism of the focusing rings, a large number of focusons will be rapidly defocused. Only a few of them will be propagated an appreciable distance from their place of origin. There-

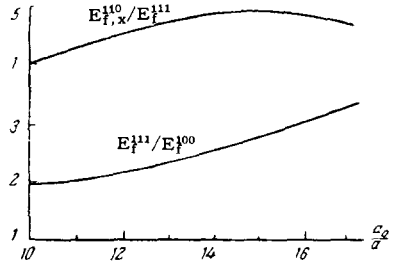

FIG. 15. Comparison of the focusing energies in different directions in a body-centered cubic metal as a function of a.

fore the number of knock-on atoms in the ⟨110⟩ direction is relatively small.

Nelson and Farmery[47], using the Born-Mayer constants obtained for tungsten, obtained the following values for the focusing energy and the number of collisions in focusons in the ⟨111⟩, ⟨100⟩, and ⟨110⟩ directions:

$$E_f^{111} = 600\,\text{eV}, \quad E_f^{100} = 200\,\text{eV}, \quad E_f^{110} = 2700\,\text{eV},$$
$$n_f^{111} = 150, \quad n_f^{100} = 20, \quad n_{f,x}^{110} = 30.$$

Figures 15 and 16 show the limiting energies at which focusing is observed and the maximum number of collisions in focusons in the ⟨111⟩, ⟨100⟩, and ⟨110⟩ directions for different values of a_0/a.

6. FORMATION AND PROPAGATION OF FOCUSONS IN OTHER CRYSTAL STRUCTURES

Balarin[48] showed that focusing of atomic collisions is possible inside the layers of the graphite lattice in the ⟨11$\bar{2}$0⟩ directions. The smallest effective diameter of the carbon atom for which focusing is possible is 2/3 of the atomic spacing (2/3 × 1.42 Å). In contrast to face-centered cubic crystals, indirect focusing due to neighboring rows of atoms is unimportant in the layer lattice of graphite. The cutoff focusing energy is several tens of electron volts.

7. STUDY OF ATOMIC COLLISION FOCUSING WITH HIGH-SPEED ELECTRONIC COMPUTERS

By means of a high-speed electronic computer, Gibson, Goland, Milgram, and Vineyard[16] made an analysis of radiation damage in a model of a copper crystal consisting, in the limiting case, of 998 atoms. In their calculations three Born-Mayer potentials were used of the type of (1) with different constants A and a.

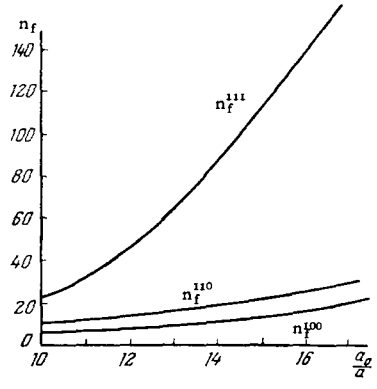

FIG. 16. Maximum number of focusons as a function of a.

The radiation damage process was initiated at a time when all the atoms of the model except one were at rest in their normal lattice sites. This one atom was given a certain amount of kinetic energy in a selected direction, as if it had just received an impact from a moving particle. In this way the paths of the atoms and the resulting damage in the crystal were determined for primary impact energies up to 400 eV.

Figure 17 shows the motions of atoms occurring in the (y, z) plane when an atom (A) is given a kinetic energy of 40 eV in a direction lying in this plane at an angle of 15° to the Oy axis.

The initial positions of atoms in the planes located immediately above and below the main plane being considered are shown by the very small dots. The large hollow circles show the atoms of the main plane at time t = 0, and the large solid dots show the positions of the same atoms at time t = 99 (the unit of time is 3.27×10^{-15} sec). The diameter of the large circles corresponds to the atomic dimensions determined by the distance of closest approach in head-on collisions between an atom with an energy of 40 eV and a stationary atom. Atoms whose trajectories are not shown undergo only minor displacements.

In Fig. 17 replacement collisions can be seen at points B and C, a vacancy remains at point A, and an

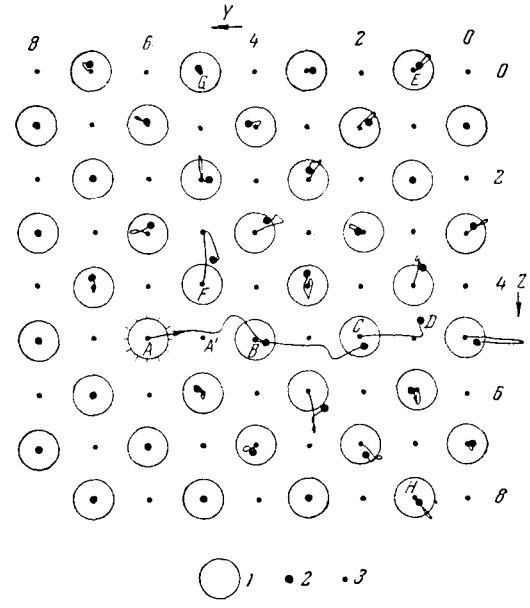

FIG. 17. Paths of atoms in a collision with an energy of 40 eV in a direction lying in the plane of the paper and at an angle $\theta = 15°$ to the Oy axis. 1 – position of atoms in the plane of the paper at time t = 0; 2 – at time t = 99. The radius of the circles corresponds to the distance of closest approach of the atoms in a 40 eV collision. The small points 3 show the projections of the equilibrium positions of atoms in the neighboring planes.

interstitial atom is formed at point D.

The regular location of the atoms in the lattice of the copper crystal model leads to focusing of atomic collisions along the ⟨110⟩ and ⟨100⟩ directions (AD, AB, FG, BH, etc.). The focusing along the ⟨110⟩ direction is essentially that which was predicted by Silsbee[9]. The focusing along the ⟨100⟩ direction occurs only as a result of the effect of neighboring rows of atoms and was not foreseen earlier. More recently the focusing in this direction has been treated by Nelson and Thompson[45], Leibfried[13] and Frere[15], using analytical methods.

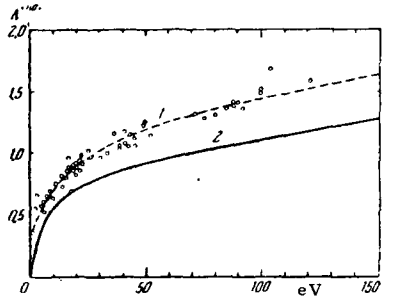

FIG. 18. Plot of Λ vs. E for the <110> direction. 1 – Computer calculations; 2 – hard-sphere approximation.

An approximate determination of the cutoff energy for focusing showed that it lies between 35 and 25 eV for collisions in the ⟨110⟩ direction and between 40 and 25 eV for the ⟨100⟩ direction (Figs. 18 and 19). The closeness of the values of cutoff energy for focusing in the ⟨110⟩ and ⟨100⟩ directions showed that both these directions are important in the propagation of radiation damage.

Since the energy loss per collision for focusing in the ⟨110⟩ direction at initial energies of the moving atoms from 3 to 400 eV does not exceed 2/3 eV, the length of the focusons can be very great. The interstitial atoms produced by such focusons will be far from the beginning of the focuson. For a focuson

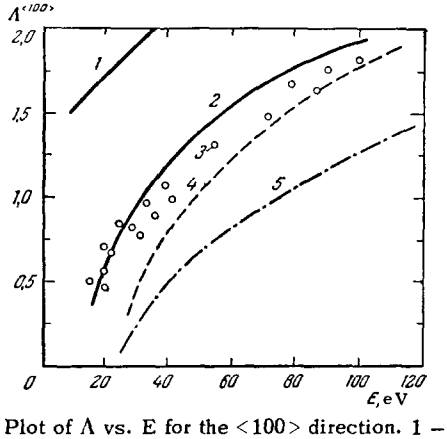

FIG. 19. Plot of Λ vs. E for the <100> direction. 1 – Calculations for an isolated row of atoms; 2 – hard-sphere approximation; 3 – computer calculation; 4 – with the Born-Mayer approximation[1]; 5 – impulse approximation.[45]

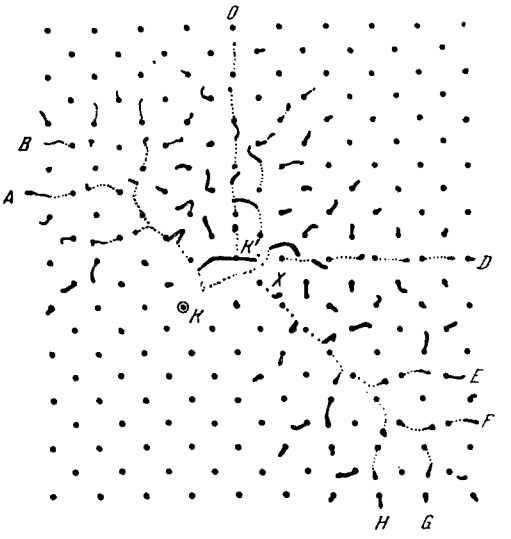

FIG. 20. An impact in the {100} plane with an energy of 400 eV at an angle of 10° to the <011> axis. Paths of atoms are shown up to a time t = 45 units. The primary atom started at K and traveled to K'. At the end of the time interval considered, the chain of collisions A, B, ... H is still in a state of active motion.

propagated along the ⟨110⟩ direction, interstitial atoms will be found at least 10 atomic distances from the beginning of the focuson, if the initial impact has an energy close to cutoff, and at least 150 atomic distances for 100 eV.

Figure 20 shows the trajectories of displaced atoms resulting from collisions with a primary atom which received an energy of 400 eV at an angle of 10° to the ⟨011⟩ direction. A primary atom from K transfers to K'. The picture refers to time t = 45; at this time the motions have propagated to the boundaries of the block, and the whole configuration is still rather far from equilibrium since this event exceeded the capacity of the calculation method used.

Focusing along the ⟨110⟩ direction, as we can see from Fig. 20, does not play the same exclusive role as in collisions with low initial energy. Since the energy considerably exceeds the maximum focusing energy for atoms in ⟨110⟩ rows, the collisions branch out along ⟨100⟩ rows, for which the energy turns out to be equal to or less than the cutoff value. The focusons in the ⟨100⟩ direction in the figure, even at the end of the calculation, remain active at A, B, C, D, E, F, G, and H. Determining the kinetic energy at these points and assuming that 7 eV per collision is lost in focusing along the ⟨100⟩ direction, we can estimate that up to 8 interstitial atoms can be formed outside the main block of the crystallite model as shown in Fig. 21. In addition another 3 atoms apparently are formed inside the block at the sites indicated in the figure. Eleven vacancies should be formed accordingly. The vacancies are located close to the point of the initial impact, and the interstitial atoms are located some distance away. Comparison of Fig. 21 with Fig. 1 shows that the region of radiation damage pro-

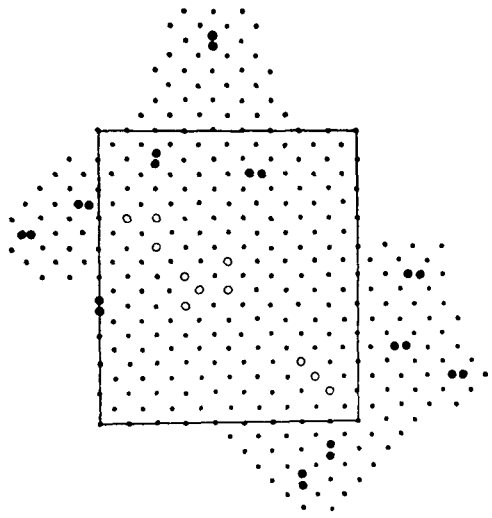

FIG. 21. An estimated extrapolation of the event shown in Fig. 20 gives a total of 11 vacancies (shown by the hollow circles) and 11 interstitial atoms (shown by the pairs of large black circles). The rectangle shows the boundaries of the crystallite used in the trial (see Fig. 20).

duced is more similar to the depleted zone of Seeger[42] than to the displacement zone of Brinkman[6], since there is nothing here which suggests the melting or the turbulent mixing of the atoms.

8. EXPERIMENTAL CONFIRMATION OF THE EXISTENCE OF ATOMIC COLLISION FOCUSING BY THE CRYSTAL LATTICE

8.1. Cathode Sputtering of Face-centered Cubic Metals

A focusing effect in atomic collision processes in metals was first observed in 1954 by Wehner[49,50], who, in sputtering single crystals of Pt, Ag, W, Mo, and α-Fe by low energy mercury ions (up to 200 eV), observed at the collector near the sputtered sample the appearance of a deposit in the form of symmetrical spots (Fig. 22). The number and location of the spots in the deposit from ion bombardment of the different planes of single-crystal silver indicated that

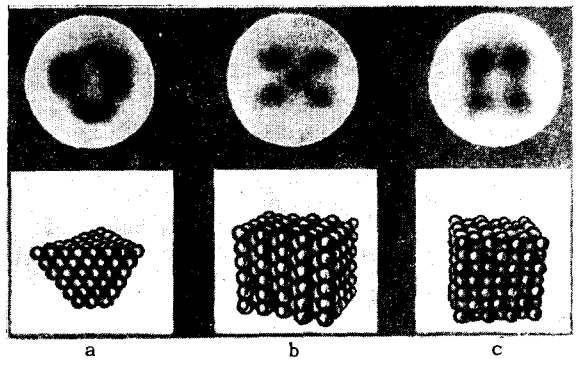

FIG. 22. Deposits obtained in sputtering different planes of a silver single crystal by bombardment with Hg ions. a) {111} plane, ion energy 100 eV; b) {110} plane, ion energy 50 eV; c) {100} plane, ion energy 100 eV.

they corresponded to close-packed rows of atoms located normal to or at some angle to the sputtered surface.

For explanation of this result Wehner[51] proposed a momentum transfer mechanism of cathode sputtering. According to this mechanism a slow ion which has collided with the surface of a metal cannot eject atoms from the metal but can only produce oscillation of atoms about their equilibrium position. The disturbance or impact wave produced by the ion is more efficiently transmitted along the close-packed rows of atoms in the crystal lattice. A certain fraction of the energy of the propagated waves can be transmitted along these rows toward the surface of the metal. Consequently a surface atom receives the greatest momentum from the neighboring atom belonging to a close-packed row. If the energy transferred to this atom exceeds its binding energy, then the atom will leave the surface of the metal and will move in the direction of close packing.

Using this mechanism, we can explain the appearance of figures of regular shape on a bombarded surface as due to preferential sputtering of material in definite crystallographic directions.

Wehner, in this same paper,[51] and several other investigators[9,52] suggested that the preferential sputtering of single crystals in particular directions should not occur if the bombardment was carried out with more energetic ions. However, in the later investigations of Yurasova and her colleagues[53,54] and of Koedam and Hoogendoorn[55] the energy of the bombarding ions was raised to 5 keV and preferential sputtering of single crystals was still observed in the four close-packed ⟨110⟩ directions for bombardment of a {100} plane (Fig.23). Furthermore, it was noted that if the ion energy exceeded 1 keV, a copper single crystal was strongly sputtered also in the ⟨100⟩ direction (which is next in density of packing to the ⟨110⟩), as a result of which there appears in the center of the deposit a new spot whose intensity increases with increasing energy.

Further investigation[56] of sputtering of the {100} plane of a copper single crystal at various energies and angles of incident Ar and H_2 ions showed that on increasing the bombarding ion energy up to 50 keV, the preferential yield of particles of the sputtered material along certain crystallographic directions (⟨110⟩, ⟨100⟩ and others) is preserved. Therefore on a collector placed parallel to the {100} surface of copper, a deposit is produced in the form of separate spots. The appearance of the deposit changes with increasing ion energy and is practically independent of the angle of incidence (from 0 to 60°). Development of relief was also observed on the {100} surface of copper in sputtering by 40 keV Ar^+ and H_2^+ ions. Four-sided pyramidal depressions characteristic of this surface were visible, similar to those observed in sputtering by slow ions. Oblique incidence of the ions

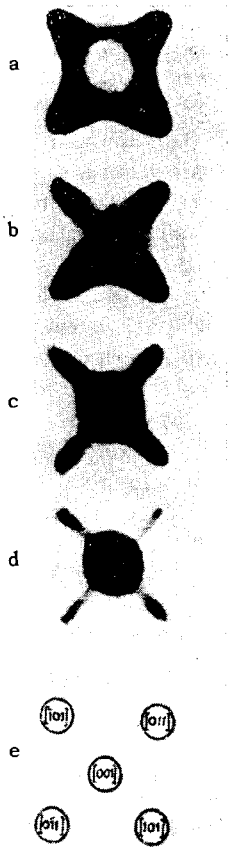

FIG. 23. Deposits obtained in sputtering a copper single crystal {100} face by normally incident Kr^+ ions. Ion energy: a) 500 eV, b) 1000 eV, c) 1500 eV, d) 2000 eV; e) theoretical location of the close-packed directions in the {110} plane.

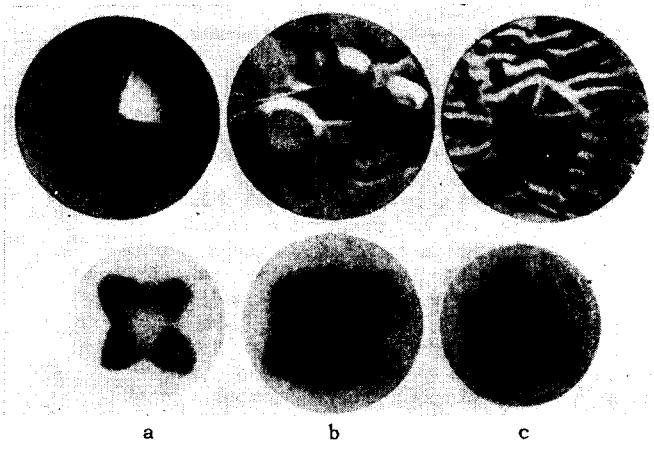

FIG. 24. Upper row: oriented depressions arising in ion bombardment of a copper single crystal on the following faces: a) {100}, b) {110}, and c) {111}; lower row: deposits obtained in sputtering of these surfaces onto a mica screen placed parallel to the sputtered face.

on the {100} surface leads, moreover, to formation of less regular figures extended in the direction of incidence of the ions. The outlines of these figures, as well as of the finer relief, are quite clear and show no visible traces of melting.

In another study Yurasova[54] has shown that the symmetry of the oriented depressions produced on the surfaces of single crystals agrees with the symmetry of the figures produced in sputtering of particles from these surfaces onto a mica screen placed parallel to the sputtered surface (Fig. 24a-c). It is particularly interesting that the appearance of additional new directions of preferential yield of atoms sputtered from single crystal surfaces, observed by Yurasova[53] and Koedam[55] for increased ion energies, leads to a change in the shape of the oriented figures on the crystal face.

Actually, Yurasova et al,[54] Wehner,[49-51] and Koedam[57] observed that in sputtering, for example, of the {111} face of copper and silver single crystals by slow ions, the preferential yield of particles occurs in the three close-packed ⟨110⟩ directions and the relief of the crystal face consists of three-sided figures. On increasing the ion energy to 300-400 eV, the preferential sputtering of material occurs not only in the three ⟨110⟩ directions but also in the three ⟨100⟩ directions coming out of the {111} face (see Fig. 24c). Correspondingly, characteristic six-sided depressions appear on the {111} face of the sputtered specimen; one of these depressions is shown in Fig. 24c.

In addition to the noble metals, preferential sputtering of particles in the close-packed directions has been observed in Ni single crystals by Wehner[58] and Koedam[59], on bombardment by ions of Hg,[58] Ar^+, Ne^+, and Kr^+[59] with energies up to 500 eV. A similar phenomenon has been observed by Perovic[60] in lead single crystals bombarded by high energy Ar^+ ions. Yurasova[44] observed an anisotropy in the sputtering of β-Co under ion bombardment.

In the bombardment of aluminum single crystals by 50 keV Ar^+ ions, Nelson and Thompson[61] observed that the density of the deposit obtained from preferential sputtering of atoms in the ⟨110⟩ direction was 2.4 times greater than in the ⟨100⟩ direction and 5 times greater than in the ⟨111⟩ direction.

An electron microscope study carried out by Haymann and Mihama[62,63] of the orientation of the planes developed in the surface of single crystals of silver, uranium, and other metals as the result of bombardment by Ar ions showed preferential development of the close-packed planes (see for example Fig. 25a and b). It was established that the set of planes developed is a function of the direction of the ion beam: not one of the developed surfaces was at an angle greater than 30° to the direction of the ion beam or to the direction perpendicular to the beam. The results obtained, when discussed from the point of view of the theory of atomic collision focusing[9], show good agreement with the predictions of Silsbee's theory.

8.2. Cathode Sputtering of Polycrystalline Face-centered Cubic Metals

The ejection of atoms in a close-packed direction under ion bombardment is observed not only in the

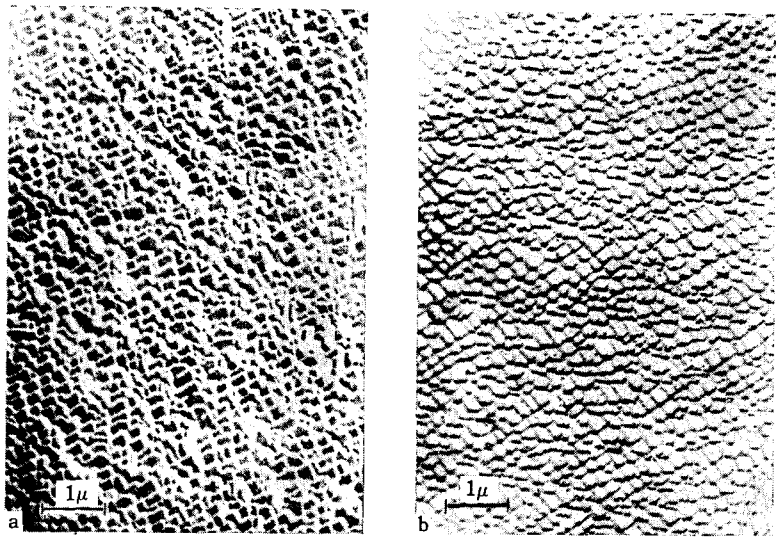

FIG. 25. Electron-microscope pictures of the {110} face of an Ag single crystal sputtered by Ar ions incident at angles of (a) 90° and (b) 60° to the sputtered surface.

case of single crystals but also for polycrystalline metal samples. Nelson and Thompson,[45] studying the sputtering of polycrystalline foils of copper, silver, and gold bombarded by 10 keV Ar^+ and Xe^+ ions from a glow discharge, observed that the distribution of sputtered material on the screen indicated preferential sputtering along the crystallographic directions ⟨110⟩, ⟨100⟩, and ⟨111⟩, which they explained by the focusing action of the crystal lattices of the bombarded metals. On bombarding surfaces of targets with {100} plane preferred orientation by an ion beam at an angle of 20° to the surface, the deposit revealed a four-fold symmetry (Fig. 26). The central spot is due to the preferential emission of atoms in the ⟨100⟩ direction; the four outer spots, which together with the central spot form a rhombic figure, are due to preferential emission of atoms in the four ⟨110⟩ directions. Figures 27 and 28 show the deposits obtained in sputtering of the surfaces of targets with {110} and {111} plane preferred orientation. Nelson and Thompson, in explaining the processes occurring in atomic collisions along close-packed directions, point out that focusing and energy transfer occur along the ⟨110⟩ direction without formation of recoil atoms, while along the ⟨100⟩ and ⟨111⟩ directions the energy transfer is accompanied by replacement of a target atom by an incident atom, as we have discussed earlier in Sec. 4.

Preferential sputtering in polycrystalline materials has been observed by Rol et al.[64] in copper,

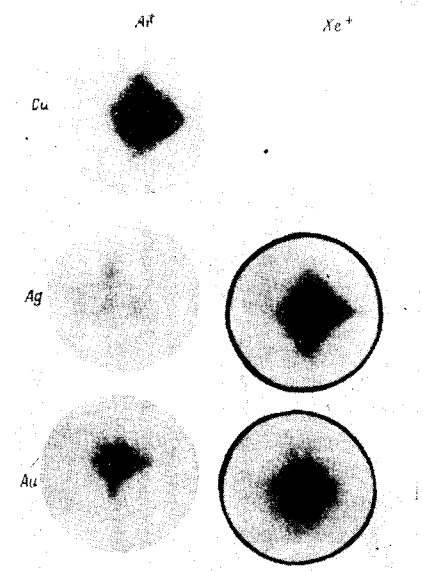

FIG. 26. Deposits obtained in sputtering Cu, Ag, and Au foils with {100} preferred orientation by Ar^+ and Xe^+ ions incident at an angle of 20°.

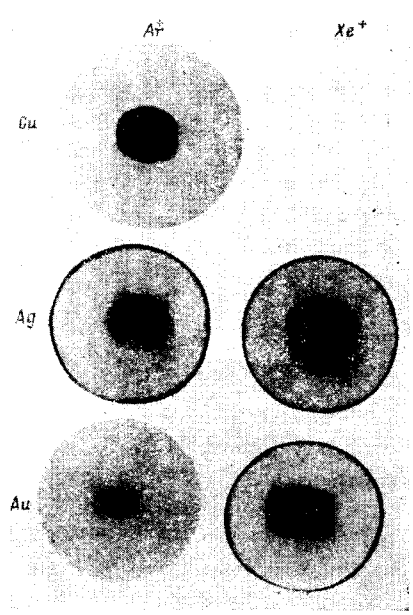

FIG. 27. The same as Fig. 26 but with {110} preferred orientation.

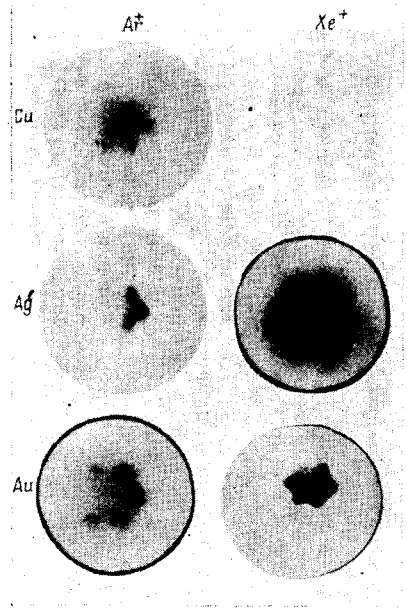

FIG. 28. The same as Fig. 26 but with {111} preferred orientation.

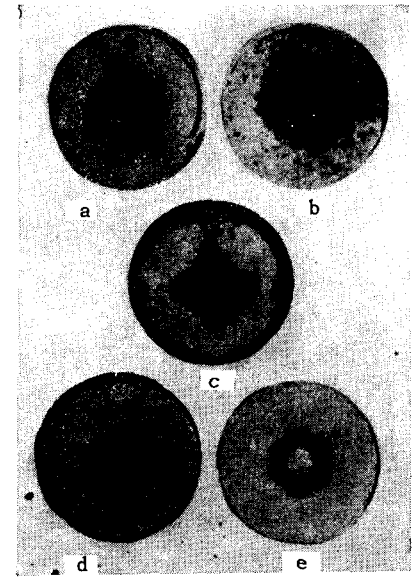

FIG. 29. Deposits obtained from proton irradiation of: a) gold; b) gold foil with random distribution of grains; c) gold foil with cubic preferred orientation of grains; d) gold foil with two preferred orientations of grains in a {111} plane in the surface; e) the same as (d) but with application of +120 V to the collector.

Koedam,[65] and O'Briain[66] in silver, by Perovic and Cobic[67] in copper and lead, and by Wehner and Rosenberg[68] in nickel and platinum.

For verification of the question whether or not the preferential sputtering of atoms in close-packed directions is a surface effect, Nelson and Thompson[45,69] performed an experiment with high energy sputtering. A polycrystalline gold foil with accurately determined crystallite orientations was bombarded by 0.3 MeV protons. They observed a preferential ejection of gold atoms from the reverse side of the target in the ⟨110⟩ direction. This is shown by the shape of the deposits obtained on the screen placed behind the target (Fig. 29). They further established that the gold is ejected from the target in the form of singly charged ions with energies 350 ± 100 eV. Since the experimental arrangement allowed them to change the energy of the bombarding protons, they were able to show that the gold ions were emitted from the target even when the protons penetrated the target only to a point of the order of 10^4 Å from the back side. This allowed them to determine the range of focusons in gold under high energy bombardment.

8.3. Cathode Sputtering of Body-centered Cubic Metals

For crystals with a body-centered cubic lattice the focusing condition $\alpha < 2$ can be fulfilled not only in the closest-packed direction ⟨111⟩, but also in the ⟨100⟩ direction although that is less favorable. Therefore sputtering of material is to be expected in the second most closely packed direction ⟨100⟩ for bcc crystals, which has been observed by Yurasova and Sirotenko[44] and Nelson and Farmery.[47]

Figures 30a and b show the autographically recorded deposits obtained by Nelson and Farmery[47] from a single crystal of tungsten on bombardment of the {111} and {110} faces by 50 keV Ar^+ ions. The spots in the deposit correspond to the preferential emission of atoms in the direction parallel to the {110} plane. Quantitative measurements showed that in the ⟨111⟩ spot together with its three auxiliary spots there are twice as many tungsten atoms as in the ⟨100⟩ spot and twelve times as many as in the ⟨110⟩ spot.

The general appearance of the spots in the deposits obtained by Nelson and Farmery[47] from the bombardment of molybdenum is similar to the case of tungsten, including the position of the main and auxiliary spots. The intensity of the ⟨111⟩ spot for molybdenum, as for tungsten, was two times greater than for the ⟨100⟩ spot, but only eight times greater than the intensity of the ⟨110⟩ spot.

The authors assert that if the process of atom ejection can be explained by the arrival of focusons at the surface, the results presented above imply that the initial momentum obtained by an atom of a crystal is dispersed in the ⟨111⟩, ⟨100⟩, and ⟨110⟩ directions at the end of the range of the bombarding particle. The oval shape of the deposited spots produced by atoms emitted from tungsten in the ⟨110⟩ direction is explained by Nelson and Farmery as due to astigmatism of the focusing "lens" in this direction in body-centered cubic lattices, which we have discussed in Sec. 5.

A possible explanation of the auxiliary spots in Fig. 30 was given by Nelson and Farmery. They assumed that focusons reaching the metal surface not only eject atoms but also create surface vacancies. Because of these vacancies, strains are produced in the

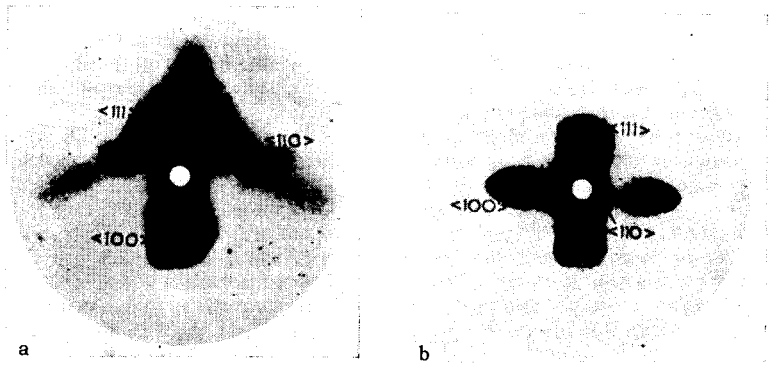

FIG. 30. Deposits obtained in sputtering of a W single crystal by 50 keV Ar^+ ions: a) the {111} face, b) the {110} face.

surrounding lattice, leading to a relaxation of the neighboring atoms. Figure 31 represents the location of atoms in one of the three {110} planes intersecting the {111} surface. It is assumed that V is a vacancy produced in the surface layer. The nearest neighbor atoms, including atom A, undergo relaxation and move toward V by an amount δ. Then, if a focuson is propagated in the ⟨111⟩ direction to atom A, as a consequence of the relaxation the ejection of atom A will occur at a small angle η to the true focusing direction. Relaxation of the next nearest neighbor atom will also affect the deviation of the ejected atom, but by an amount much less than η. In the approximation of hard spheres of diameter $D^{111}/2$ the deviation angle η will be given approximately by

$$\eta = \frac{2\delta}{D^{111}/2}. \qquad (47)$$

The values of η measured from the deposits obtained from ejection of tungsten atoms in the ⟨111⟩ direction are ~ 10°, which gives a relaxation of the atoms of approximately 8%. This value of relaxation is close to the theoretically calculated value of ~ 6% for tungsten and molybdenum.[70,71]

Bands which are observed in the deposition patterns of atoms ejected from tungsten are considered by Nelson and Farmery to be due to the emission of recoil atoms channeled between neighboring {110} planes. The distance between these planes is large compared to other planes, and therefore the space between them is relatively transparent for recoil atoms.

Similar bands observed in the deposition patterns from sputtered face-centered cubic crystals have also been explained by Nelson and Thompson[72] as due to channeling of recoil atoms between neighboring {111} planes.

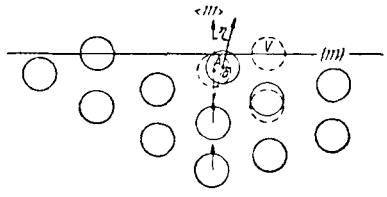

FIG. 31. Effect of a surface vacancy on a series of atomic collisions in the <111> direction.

Preferential sputtering of atoms in close-packed directions in body-centered cubic crystals has been observed by Yurasova[44] in single crystals of Fe, Cr, and W, and by Wehner and Rosenberg[68] in polycrystalline Mo and Fe.

8.4. Cathode Sputtering of Diamond Structure Metals

In the sputtering of single crystal spheres of germanium and of indium-antimony alloy on bombardment by 1 to 10 keV Kr ions, Yurasova and Sirotenko[44] observed deposition spots corresponding to sputtering of material in the ⟨110⟩ and ⟨100⟩ directions. However, in comparison with the spots obtained from bcc and fcc crystals, the spots for Ge and InSb were less distinct. The appearance of these spots, in the opinion of the authors, cannot be explained by the focusing effect. The focusing condition $\alpha < 2$ cannot be fulfilled for any one of these directions in this case, since if it were the spheres of two neighboring atoms, spaced a distance of $a\sqrt{3/4}$ along the ⟨111⟩ direction, would overlap.

Koedam[57] did not observe sputtering in preferred directions in the bombardment of Ge single crystals. However, an electron diffraction study of the target showed that amorphous layers were formed on its surface during the bombardment. On heating the Ge to 500°C the crystal structure of the surface layer was partially restored, which led to appearance of a weakly expressed preferential sputtering direction. Anderson,[73,74] in bombardment of the {100} and {110} surfaces of germanium and silicon single crystals by Hg, Ar, and Ne ions, observed preferential ejection of atoms corresponding to the ⟨111⟩ and ⟨100⟩ directions, which can perhaps be explained by the presence of a large number of atoms in interstitial positions on the surface of the bombarded specimens. From the results of his experiment Anderson concluded that focusons do not play as great a role in crystals of the diamond structure as in face-centered and body-centered cubic crystals. The focusons can be formed and propagated only in thin surface layers of the bombarded crystals. The structure of the surface layers evidently approximates a bcc structure, since it would otherwise be impossible to explain the ejection of atoms in the ⟨100⟩ direction.

8.5. Cathode Sputtering of Hexagonal Metals

Yurasova and Murinson[75] studied the cathode sputtering of a cylindrical single crystal of zinc whose end plane was the basal plane {001}. The most closely packed directions, ⟨110⟩, which lie in the basal plane, were perpendicular to the cylinder axis. The sputtering was carried out in a Kr plasma at a voltage of 1.2—1.3 KV. The appearance on the spherical collector after the sputtering of six spots located along a great circle of the sphere at equal distances from each other and corresponding to the close-packed ⟨110⟩ directions indicates that for crystals with a hexagonal lattice preferential sputtering of material occurs in the close-packed direction, as in cubic crystals.

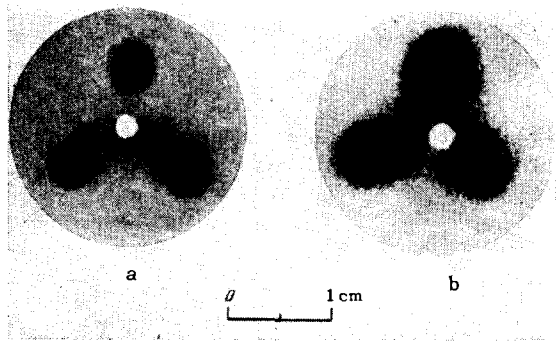

FIG. 32. Deposit obtained in sputtering the {111} face of a gold single crystal by 43 keV Ar^+ ions at target temperatures of: a) 370°K and b) 1170°K.

8.6. Effect of Nuclear Charges of Moving and Stationary Particles on Cathode Sputtering

According to an analysis made by Bohr,[76] the interaction potential between moving and stationary particles is given by

$$V(r)=\frac{Z_1Z_2e^2}{r}\exp\left(-\frac{r}{a}\right), \qquad (48)$$

where Z_1 and Z_2 are the nuclear charges of the moving and stationary particles, a is the screening constant, and r is the distance between the centers of the moving and stationary particles. It is evident from (48) that, generally speaking, the effective hard-sphere diameter r depends not only on E but also on the nuclear charge of the moving and stationary particles Z_1 and Z_2. The greater Z_1 and Z_2, the greater is r. It follows from this that focusing should occur best of all for materials with high Z. This is in agreement with the experimental results obtained by Yurasova and Sirotenko[44] on the sputtering of tungsten and chromium. Actually tungsten and chromium have approximately the same value of sputtering coefficient and the lattice constant of tungsten is even larger than that of chromium, but nevertheless the spots in the deposition pattern of tungsten are more distinct than for chromium. This may be due to the fact that the radius r/2 of tungsten is significantly larger, other conditions being equal, than for chromium (since $Z_W > Z_{Cr}$).

8.7. Effect of Specimen Temperature on Cathode Sputtering

Nelson and Thompson[77] studied the distribution of the deposits obtained in sputtering of the {111} surface of a gold single crystal by 43-keV Ar^+ ions, as a function of the crystal temperature over the range 80—1170°K. They observed a preferential yield of sputtered particles in directions close to the ⟨100⟩ axis of the crystal. Fig. 32a shows a deposition pattern obtained from a specimen heated to 370°K, and Fig. 32b, from a specimen heated to 1170°K. The spots in both patterns correspond to the three ⟨110⟩ directions of preferential sputtering of gold atoms.

Increase in the temperature of the specimen increases the size and density of the spots. Quantitative measurements of the density and angular distribution of the sputtered deposits on the screen, carried out by irradiation of the deposits by a flux of thermal neutrons and subsequent autoradiography, showed a linear rise of the mean squared angle of deviation ψ^2 with temperature up to 800°K, and above that a more rapid increase (Fig. 33). The authors also calculated the number of focusons formed in gold at different temperatures during the bombardment (Fig. 34).

The experiments of Yurasova[78] on sputtering of the {100} and {111} faces of a copper single crystal as a function of temperature showed that preferential sputtering in the close-packed directions is observed over a wide temperature range: from 103°K, obtained by cooling the specimen with liquid nitrogen, up to a temperature of 1223°K where the sample vaporized rapidly. It was observed that the directional yield of sputtered particles was particularly striking at temperatures up to 723°K. On cooling the specimen with

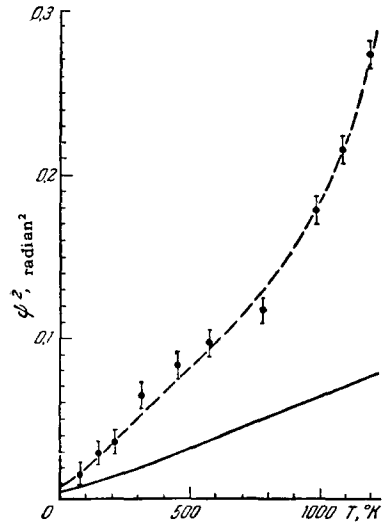

FIG. 33. Mean squared angle of deviation from the <110> direction, ψ^2, as a function of target temperature. The upper curve shows the experimental results and the lower curve the theoretical calculation.

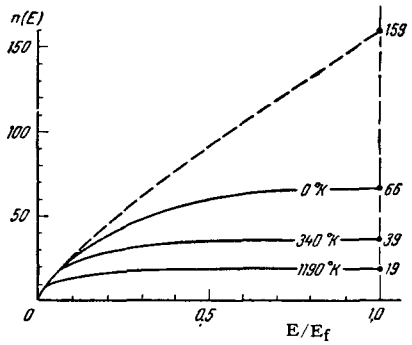

FIG. 34. The number of collisions in a focuson as a function of the energy, for different target temperatures. The upper curve refers to the hypothetical case of a stationary lattice.

liquid nitrogen the sharpness of the individual spots in the deposition pattern was practically unchanged. Increasing the temperature of the single crystal up to 1223°K resulted in an increase in the general background in the deposition pattern and in a considerable increase in density and size of the central spot (Fig. 35).

In order to remove any doubts as to the mechanism of preferential sputtering, Yurasova[78] carried out supplementary experiments on the thermal evaporation of a copper single crystal at a temperature of 1223°K. These experiments showed that, independently of the initial state of the surface (after polishing, ionic etching, or heating of the crystal to a high temperature) the deposit on the screen due to evaporation of material from the {100} face was distributed not in the form of individual spots but with a conical distribution (Fig. 35e). On subsequent ion bombardment of the same surface region, the characteristic shape of deposit was formed without any change.

Yurasova and her colleagues[78] explain the changes in the sputtering pattern obtained on increasing the temperature by a weakening of the binding of the atoms in the lattice with increased temperature and an increase of the thermal oscillations of the atoms, which deteriorates the focusing conditions; the sputtered atoms emerge from the crystal surface with a larger deviation from the close-packed direction than at low temperatures. Therefore the spots in the close-packed direction become less sharp. Furthermore, the weakening of the binding of the atoms in the lattice may have the result that the momentum required for ejection of atoms from the surface can be transferred from deeper layers of the crystal, just as this occurs on increasing the energy of the bombarding ions.[56] In this case the yield of particles from the surface has a somewhat different mechanism than at low temperatures and energies, and in particular the yield of atoms (or the momentum transfer) has a higher probability along the shortest path from the place of excitation to the surface than in a direction inclined toward the surface, even along close-packed rows. In this way we can explain the strengthening of the

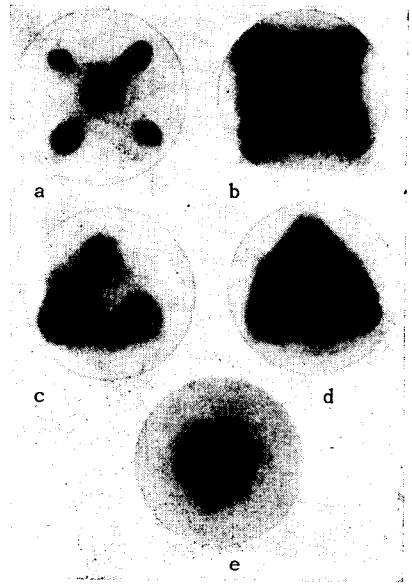

FIG. 35. Deposits obtained in sputtering of the {100} face (a and b) and the {111} face (c and d) of a copper single crystal at different temperatures: a) 100°C; b) 950°C; c) 100°C; d) 800°C; e) pattern obtained from the evaporation of material from a {100} face at 950°C.

central spot in comparison with the outer spots which is observed for sputtering of the {100} face on increase of the crystal temperature (Fig. 35). This assumption is also confirmed by the fact that in the sputtering pattern from the {111} face at 823°K (Fig. 35) there is also observed a central spot which at 1223°K exceeds the other spots in density and becomes appreciably broader than any of them.

Studying the sputtering of tungsten at different temperatures, Yurasova and Sirotenko[44] observed that at 1300°C the spots were more sharply bounded than at 200—300°C. This phenomenon is explained as follows. On increasing the temperature of the specimen two processes occur: removal of various contaminants from the surface, which results in increased clarity of the picture, and an increase of the oscillations of the atoms about their equilibrium positions, which should lead to a reduction in the sharpness of the deposit pattern. Probably at a temperature of 1300°C in tungsten the first process prevails over the second.

Molchanov, Tel'kovskiĭ, and Shakh-Melikova[79] also studied the effect of temperature (from 150—700°K) on the angular distribution of the sputtered particles from a copper single crystal during irradiation by 27 keV Ar ions normal to the {100} surface. They observed that with increasing temperature the width of a spot in the deposit decreases somewhat and then grows slightly. However, the authors consider that the current density in the ion beam and the value of radiation dosage in their experiments might have been insufficient to produce distortions capable of affecting the angular distribution.

8.8. Study of the Angular Distribution of Sputtered Particles in the Bombardment of Metals by Ion Beams

Study of the angular distribution of sputtered particles is of more than solely scientific interest. Recognition of the regularities of metal sputtering by ions arriving at angles near grazing incidence is very important for solution of many technical problems, for example, in the study of the effect of sputtering on the operation of ion engines,[19] and is vital for explaining the mechanism of cathode sputtering.[80]

We know that the condition for focusing of atomic collisions along any crystallographic axis is determined by the ratio of the energy-dependent effective atomic diameter to the interatomic distance. In some crystals the distances between atoms along different axes are greatly different, so that focusing is possible along some axes and impossible along others. By studying the anisotropy of the sputtering coefficient of such crystals, we can draw certain conclusions about the effect of focused collisions on sputtering.[80]

Molchanov, Tel'kovskiĭ, and others[81,82] established that the sputtering coefficient increases with increasing angle of incidence of the ions on the target inversely as the cosine of the angle of incidence. The independence which they observed of the distribution of sputtered atoms on the mass and energy of the ions serves as indirect confirmation of the transfer of energy by focused collisions.

The anisotropy in the sputtering of zinc, which has a hexagonal close-packed lattice, was studied by Balarin, Molchanov, and Tel'kovskiĭ.[80] For hexagonal crystals the ⟨100⟩ directions in the basal plane will be focusing directions; in other directions, particularly ⟨210⟩, indirect focusing is possible from the action of neighboring rows of atoms, but energy transfer in these directions is rapidly attenuated. Experimental studies have confirmed the existence of focusing in hexagonal crystals and have shown that on the average the sputtering coefficient is larger for a larger distance between corresponding atomic layers, i.e., for a smaller packing density of an axis. The close correspondence between the angular dependence of the sputtering coefficient and the angular distribution of sputtered material,[83] in the opinion of the authors, indicates a connection between the sputtering coefficient anisotropy and focused collisions in the specimen.

An irradiation of the basal plane of a single crystal by 30 keV Ar^+ ions, carried out by Molchanov, Soshka, and Faruk,[84] also revealed a directional yield of particles along the ⟨101⟩ axis, as the result of which six deposition spots occurred on the collector. The half-width of the angular distribution of particles sputtered in the ⟨101⟩ direction was 24°. Thus, as in the case of cubic crystals, hexagonal structures have a close correspondence between the angular distribution of sputtered particles and the dips in the angular dependence curve of the sputtering coefficient. A large number of experiments on cathode sputtering[85,86] have shown that these dips are observed only when the ion beam direction coincides with a close-packed direction in the irradiated metal.

9. EXPERIMENTAL CONFIRMATION OF THE PART PLAYED BY FOCUSING PROCESSES IN RADIATION DAMAGE IN METALS

9.1. Electron-microscope Observation of Radiation Damage

Brandon and Bowden[88,89] made an electron-microscope study of thin gold foils before and after their bombardment by 75—100 eV Ar^+ ions. The maximum energy transferred to the gold atoms was 57% of the maximum energy of the bombarding ion. They observed numerous defects in the crystal structure, whose nature depended strongly on the crystallographic orientation of the bombarded foils. The density of defects turned out to be greatest for low temperature bombardment (241°K). For bombardment at 295°K they observed lines formed by dislocation loops up to 500 Å in size along the ⟨111⟩ direction (Fig. 36). Since the dislocation loops formed as the result of the bombardment were observed at a depth of 150 Å under the surface of the foil, and the Ar ions could penetrate only one or two atomic layers beneath the surface, the authors concluded that radiation damage at such a depth below the surface was due to focusing collisions of atoms.

FIG. 36. Electron-microscope photograph of a gold foil irradiated by 80 eV Ar ions. Dislocation loops are distinctly visible along the <111> direction.

Amelinckx and colleagues[90,91] subjected platinum foils to irradiation by fission fragments and alpha particles and then studied them in a transmission electron microscope. They observed preferential formation of prismatic loops at specific boundaries, especially along coherent twin boundaries (Fig. 37). The mechanism of formation of these defects becomes clear if we consider a focusing sequence of collisions along the ⟨110⟩ direction in the irradiated platinum. In a platinum crystal the ⟨110⟩ direction on one side of a twin is parallel to the ⟨114⟩ direction in the other

FIG. 37. Preferential formation of defects at coherent twin boundaries in a platinum foil irradiated by fission fragments. The plane of the foil is a {110} plane.

part of the crystal. On arriving at the internal surface of the twin, the focusing collisions suddenly are defocused, and since they deliver to this point energy sufficient for production of displacements, they begin to form defects at the twin boundary. Figure 38 shows a coherent twin boundary located perpendicular to the plane of the drawing—the {110} plane. There is clearly a high probability that the chain 1, 2, 3 will produce displacement of atom 5. Furthermore, atom 3 will almost certainly be ejected from the row 1, 2, 3. This shows that such chains of focused collisions, on defocusing at a coherent twin boundary, will lead to preferential formation of defects along this boundary. The loops apparently originate at clusters of vacancies remaining from previous processing of the foil, or else the vacancy clusters lead to a decrease in the focused collisions and consequently to an increase in defects in the structure.

9.2. Direct Observation of Radiation Damage

By using transmission electron microscopes with resolution as good as 10 Å to study thin metallic foils subjected to irradiation, we can observe large clusters of radiation defects. However, many processes occurring in the bombardment of metals by nuclear particles cannot be resolved. In particular, the electron-microscope method does not provide the possibility of studying such defects as single vacancies and interstitial atoms.

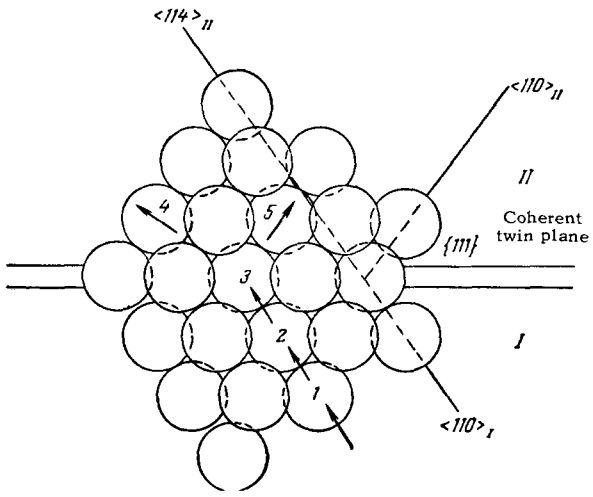

FIG. 38. Diagram of the propagation of atomic collisions leading to preferential formation of defects at coherent twin boundaries in a platinum foil irradiated by fission fragments.

Only with the aid of the ion projector, which has a resolution of 2—3 Å, has it been possible, in the work of Müller[93] and Brandon and Wald[94], to observe point defects produced in tungsten by α-particle irradiation (at the time of observation in the projector).

Müller's experiments[93] have shown that each incidence of an α particle is visible and that the defects are visible only at the point of exit. Displacement of roughly 15—30 atoms occurs in a region of diameter about 50 Å. Two thirds of the displaced atoms appear to be interstitial atoms directly under the surface, and about one third of the displaced atoms disappear from the surface. This could be the end of a wedge-shaped displacement zone at the surface. In approximately half of the collisions observed by Müller, simultaneously with major damage in the region of the particle's exit, small defects appear, for example, from one to three interstitial atoms located in a close group, separated from the place of the main damage by a distance of up to half the radius of the point. Müller considers that the small defects result from the high energy impact produced by secondary atoms which have branched off from the main track, or else are the result of energy transfer by sequences of focused collisions. We must also note that craters are never observed in α-particle irradiation, although we would expect them if the temperature rose in the displacement zone.

Figure 39 shows photographs of the same area of a tungsten surface before and after the incidence of an α particle. The photographs were obtained by Brandon and Wald[94] who bombarded a tungsten point in a projection tube with 5 MeV α particles. The atoms ejected from the surface are marked by points in Fig. 39a. Atoms which have moved to new positions on the surface are similarly marked in Fig. 39b. It is evident that within a solid angle of $\sim\pi$, about 40 atoms have been ejected. If we assume that every

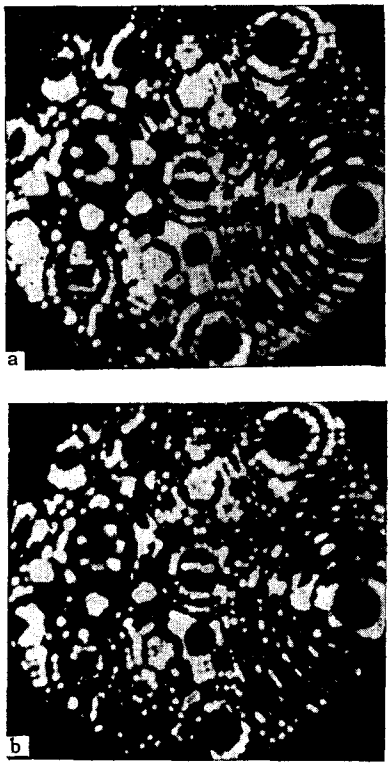

FIG. 39. a) Picture of tungsten atoms in an ion projection tube, obtained before the incidence of an α particle on a tungsten point. The atoms ejected as a result of the collision are marked with dots. b) Picture of the same tungsten atoms after collision with an α particle.

fifth site in the crystal lattice is visible, the total number of sequential collisions resulting from the initial α-particle impact must be about 800. Damage to the structure on the surface is observed at a distance of more than 200 Å from the point of the initial collision. This distance is considerably greater than that which would be traversed by an atom which received the initial impact. Figure 40 shows a diagram of consecutive displacements resulting from incidence of an α-particle, which helps to understand the picture obtained. The momentum received by a metallic atom in a collision with the α-particle is successively transferred by focused atomic collisions along close-packed $\langle 111 \rangle$ and $\langle 100 \rangle$ rows to the surface on the other side of the tungsten point. As a result of the removal of the atoms at the ends of these rows, vacancies are formed which are visible in Fig. 39b as dark spots.

10. EXPLANATION OF THE CHANGES IN THE PROPERTIES OF METALS UNDER IRRADIATION, IN TERMS OF ATOMIC COLLISION FOCUSING

In a study of the energy dependence of radiation damage produced in pure copper and copper with impurities of Be, Ag, or Au by electron bombardment at a temperature of 4.2°K, Sosin[95] established that the experimental results are in good agreement with the mechanism of focused collisions along close-packed

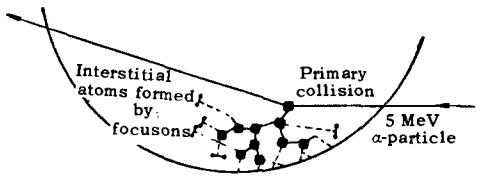

FIG. 40. Diagram explaining the process of defect formation in a tungsten point as the result of a collision with a single α particle. The surface defects are formed: 1) as the result of secondary collisions, 2) by focusons.

directions. With this mechanism it has been possible to explain the occurrence of displacements at a relatively large distance from the place of the initial electron-atom collision, which cannot be explained at these temperatures by other mechanisms.

The mechanism used by Sosin can be applied to explanation of the hardening effect observed by Makin and Blewitt[96] in copper single crystals under electron bombardment. According to their hypothesis, the most probable factor responsible for the hardening is the formation of strongly diffused obstacles in the crystal lattice which block the motion of dislocations; these obstacles must be extremely small since they are not observed under the electron microscope. According to the mechanism of focused collisions, such obstacles to the motion of dislocations can appear as the result of the intersection of focusons with dislocations.

Leibfried,[10] in discussing the work of Thompson, Holmes, and Blewitt[97] on the effect of low temperature neutron bombardment on the mechanical properties of a copper single crystal, used the mechanism of focused collisions to explain the decrease in internal friction. In easily deformed metals such as copper, with a high dislocation density the effects of low temperature bombardment cannot be explained by the old theories of radiation damage, since the defects are immobile at such temperatures.

Billington[98] has shown that near the end of the range of secondary displaced particles in copper irradiated by neutrons, thermal spikes arise which, he assumes, lead to the appearance of small melted regions. Leibfried,[10] in evaluating the maximum temperature in the region of a possible thermal spike in copper, showed that regions of melting cannot occur in this case since the temperature will reach only 500°C. The residual energy of the displaced atom will be propagated throughout a large volume by means of focusons.

At the same time a study by Thompson[99] of thermal spikes produced in gold on bombardment by 43 KeV Xe^+ and Ar^+ ions showed that the atoms deposited on the screen are obtained as the result of evaporation from a region of local heating. These regions arose from thermal spikes giving temperatures up to 1750°K. It was observed that the radius of the region of local heating ($\sim$ 110 Å) depends to a

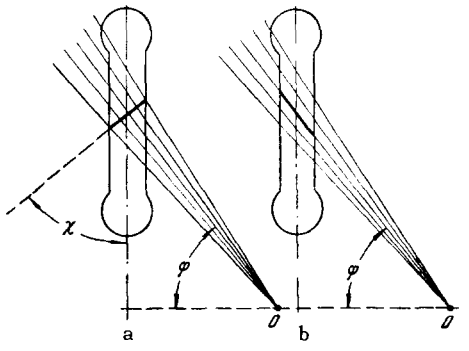

FIG. 41. Position of the basal plane of single-crystal specimens of zinc with respect to the particle flux emitted by a source located at point O. a) Transverse position of the basal plane; b) longitudinal position, after rotation of the specimen about its own axis by 180°.

greater degree on successions of focused collisions than on the energy of recoil atoms.

Focusing processes can affect the change of mechanical properties in metal single crystals with a hexagonal lattice if they are appropriately oriented with respect to the bombarding particles. As an example we can cite the experiments of Troitskiĭ and Likhtman[100] on electron and γ-ray bombardment of zinc single crystals in a brittle state. Numerous experiments carried out by them on the stretching of amalgamated zinc single crystals subjected to radiation during the process of deformation showed that the orientation of the basal plane of the crystal with respect to the direction of the radiation is very important. When the basal plane is perpendicular to the particle flux (Fig. 41a), a significant embrittlement is observed, and when the basal plane is parallel to the flux (Fig. 41b) an increase in ductility, i.e., ultimate elongation, occurs. This phenomenon in zinc crystals also occurs under conditions of natural cold brittleness (at −196°C).

According to the theories proposed by the authors, one possible explanation of the observed phenomenon is the development of obstacles in front of the moving dislocations for the case of the basal plane perpendicular to the beam, which leads to a rapid pile-up of dislocations in front of these obstacles and even to the formation of a brittle fracture. From our point of view, such obstacles can arise from focused atomic collisions which can produce Frenkel defects on intersecting dislocations and thereby retard their motion.

In connection with the experiment of Troitskiĭ and Likhtman we can suppose that the acceleration of creep in cadmium single crystals due to α-particle bombardment of their surfaces, which was observed by Andrade,[101] can be explained by appropriate orientation of the specimen with respect to the α-particle beam. Garber and Gindin,[102] in discussing the results of this work, note that the intensity of irradiation and the depth of penetration were so insignificant that up to this time the existence of this effect has been a source of astonishment. The negative results obtained by Makin[103] in an attempt to reproduce this experiment with more intense irradiation can be explained, in our opinion, by the fact that the orientation of the crystals with respect to the beam of bombarding particles was not reproduced.

As Seitz[104] has recently suggested, focusing effects can play an important role in order-disorder transformations in alloys composed of atoms with almost equal masses, for example, copper-zinc.

It is possible that the ordering observed by Dauntreppe et al[105] in an alloy of 50% Fe - 50% Ni under neutron irradiation in a magnetic field can be explained by atomic collision focusing. In fact the direction of the magnetization which resulted in uniaxial anisotropy coincided with the ⟨100⟩ and ⟨110⟩ directions.

Gonser[106] explains the radiation-induced expansion of α-U and related phenomena on the basis of atomic collision focusing (Fig. 42). He considers that the transition observed at high temperatures from anisotropic radiation-induced expansion to isotropic expansion is due to the defocusing of atomic collision sequences.

11. EXPERIMENTAL METHODS OF STUDYING ATOMIC COLLISION FOCUSING

11.1. Investigation of Cathode Sputtering in a Glow Discharge

A considerable number of papers[107-109] have been devoted to the physics and technology of producing glow discharges. In order to obtain a glow discharge specifically for investigation of cathode sputtering, the following experimental conditions must be fulfilled.[110]

1) The mean free path of the ions and the sputtered atoms must be larger than the dimensions of the apparatus to avoid reverse diffusion of the sputtered

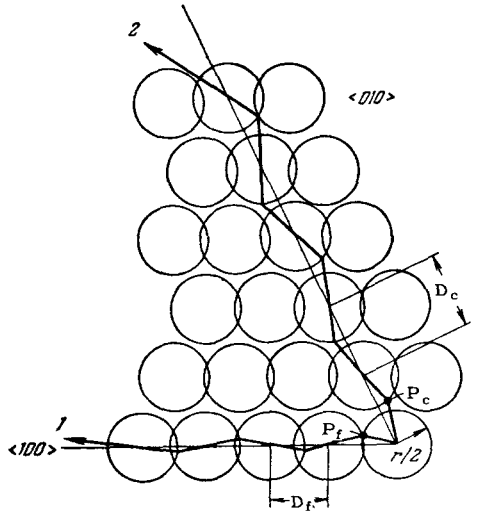

FIG. 42. Formation of focusons and crowdions in α – U.

atoms to the target and to guarantee strictly defined ion energies. These conditions can be fulfilled in a discharge at a sufficiently low pressure.

2) The ion current density should be high and the residual gas pressure should be low in order to avoid contamination of the surface.

3) To secure normal incidence of the ions, the target should be rather large and without sharp edges.

4) The voltage drop in the discharge should be relatively low in order to avoid formation of multiply charged ions.

5) The angle of incidence of the ions on the target should be well defined.

The collision energy of the ions in a glow discharge is ordinarily determined by the negative voltage applied to the target with respect to the anode.

The sputtering yield (atoms/ion) can be found by measuring the decrease in weight of the target, W (grams). Then, knowing the ion current I (amperes) and the time of sputtering t (sec), we can obtain the sputtering yield

$$\gamma = 10^6 \frac{W}{AIt}, \qquad (49)$$

where A is the atomic weight.

A rather sensitive method of determining the loss of material from sputtering is to weigh the target in a quartz microbalance, which permits detection of a change in weight of the order of 0.14 ± 0.05 micrograms. The weighing is carried out in vacuum at a pressure of 10^{-9} to 10^{-10} mm Hg.[111]

At high bombarding ion energies, and also if the material being studied has a low melting point, the target can be cooled either by blowing air through a hollow target holder[112] or by circulated water or liquid nitrogen.

Figure 43 shows the design of the apparatus used by Wehner[51] in his study of the sputtering of different metals by 300 eV Hg ions, with an ion current of 10 mA/cm² from a high density plasma produced in a glow discharge.

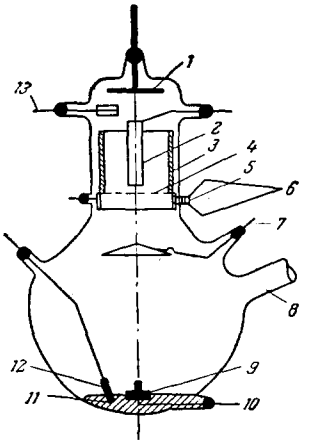

FIG. 43. Discharge tube. 1 – Reflector; 2 – target; 3 – glass collector; 4 – graphite grid; 5 – stainless steel ring; 6 – plastic spacers; 7 – auxiliary anode; 8 – to vacuum pump; 9 – cathode spot anchor; 10 – cathode; 11 – mercury; 12 – ignitor electrode; 13 – anode.

Sputtering by high energy Hg ions (4–15 keV, with an ion current density at the target of 0.32 mA/cm² at 4 keV and 2.8 mA/cm² at 15 keV) was carried out by Wehner and Rosenberg[68] in the apparatus shown schematically in Fig. 44. In both sets of apparatus the glow discharge utilized liquid mercury cathodes.

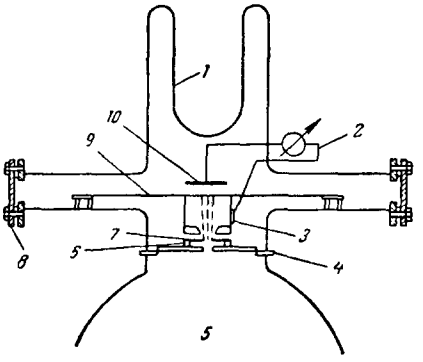

FIG. 44. Apparatus for sputtering of metallic targets by Hg ions from a glow discharge. 1 – Liquid nitrogen trap; 2 – high voltage, 4–15 kV; 3 – accelerating ring; 4 – grid at potential of +15 V; 5 – region of glow discharge; 6 – glass ring; 7 – anode potential of +22 V; 8 – means of translation in a plane; 9 – target foil with magnet; 10 – collector plate.

Nelson and Thompson,[45] in sputtering metals by Ar^+ and Xe^+ ions, used a 10 kV glow discharge between a cylindrical anode and a plane cathode. The ion beam emerging through a cylindrical slit in the cathode (1 mm in diameter and 10 mm long) was focused onto the target. The ion currents obtained in this apparatus were 15 μA for Ar and 5 μA for Xe.

11.2. Study of Cathode Sputtering by Means of Ion Guns

Use of ion guns for study of metallic sputtering has a number of advantages over sputtering in the plasma of a glow discharge, where the number and energy of the ions and their angle of incidence on the target cannot be exactly determined.[113-115]

Figure 45 shows a diagram of the experimental ap-

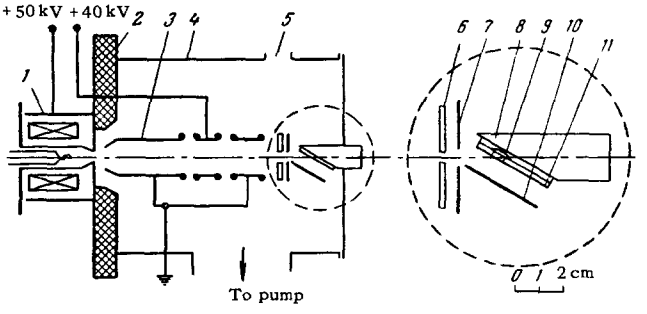

FIG. 45. Diagram of apparatus for study of cathode sputtering. 1 – ion source; 2 – insulator; 3 – single potential electrostatic lens; 4 – container; 5 – viewing window; 6 – quartz screen; 7, 10 – glass collectors; 8 – copper support; 9 – copper single crystals; 11 – mica diaphragm.

paratus used by Yurasova et al[56] for study of anisotropy in cathode sputtering. The ion beam was produced by an ion gun with a Von Ardenne source,[116] with double constriction of the plasma, as developed by a number of authors.[117]

The ion gun produced well focused beams of Ar and H ions 6—12 mm in diameter with currents up to 3 and 20 mA, respectively, at an accelerating voltage of 50 kV. The ion beam, after acceleration and focusing by a single electrostatic lens, passed through an aperture 4—8 mm in diameter in a quartz plate and hit the specimen. In front of the specimen and parallel to its working surface was placed a mica sheet or glass collector on which the sputtered particles were deposited.

Bradley and Ruedl,[118] using the sputtering apparatus shown in Fig. 46, obtained an ion beam by ionization of a neutral gas with an electron beam. The ions obtained in this way were then accelerated to 1 keV. The maximum current density reached with this apparatus was 10 mA/cm^2. The targets studied could be bombarded by ions of Ar^+, N, O, or Xe^+. The particles ejected from the target were ionized by an electron beam and then analysed.

For studying the sputtering of atoms from the reverse side of a target of polycrystalline gold foil 20—25 mg/cm^2 in thickness, with strictly defined crystallite orientation, Nelson and Thompson[45] used protons from a Van de Graaff accelerator. The accelerator gave protons from 0—0.6 MeV. The proton energy was chosen experimentally for each target. It corresponded to the minimum proton energy at which all protons pass through the target. The target temperature was held at 200°C during the irradiation. The gold atoms leaving the back side of the target were deposited in vacuum on a glass plate covered with a layer of aluminum to improve the adherence.

The method used by Nelson and Thompson and others[45,47] for studying the distribution of the deposit on the collector is of considerable interest. Since the number of sputtered atoms deposited on the collector can be very small ($\sim 10^{13}$), the density of the deposit cannot be determined photometrically. Therefore the collector with the atoms deposited on it

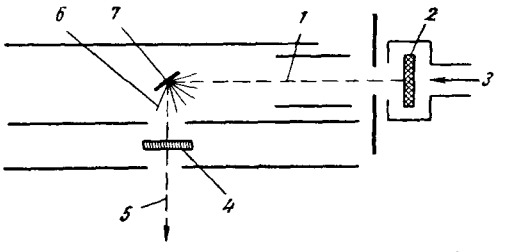

FIG. 46. Apparatus for analysis of sputtered particles. 1 – primary (bombarding) ion beam; 2 – electron beam; 3 – neutral gas; 4 – electron beam ionizing sputtered particles of the target; 5 – secondary ion beam, directed into analyser; 6 – sputtered particles; 7 – target.

was subjected to irradiation for five days by thermal neutrons in a nuclear reactor (10^{12} neutrons/cm^2-sec). The distribution of atoms in the collector deposit was then determined either by autoradiography or by a Geiger-Mueller counter.

In some studies[47,49] the targets were bombarded by ions with energies up to 50 keV obtained from the Harwell heavy ion accelerator.[119] Figure 47 shows the experimental setup for study of the effect of temperature on atomic collisions in a single crystal gold foil bombarded by Ar ions from this accelerator. The ejected atoms were deposited on a quartz collector. Heating of the target to 1170°C was achieved by bombardment with a 2 kV electron beam with a maximum current of 2 mA (Fig. 47b). Pictures of the deposit which resulted from the sputtering were obtained by autoradiography.

11.3. Study of Cathode Sputtering with an Electron Microscope

Haymann,[63] using equipment mounted on the base of a vertical electron diffraction apparatus, studied the selective sputtering of metallic crystals on bombardment by Ar ions with controlled energies from 0 to 20 keV, and an ion beam density of 2 mA/mm^2 obtained from an ion gun mounted in the column of the diffraction apparatus. This equipment allowed visual observation of the sputtered targets and photographing of their surfaces with a magnification up to 2000× through a special optical microscope mounted in the

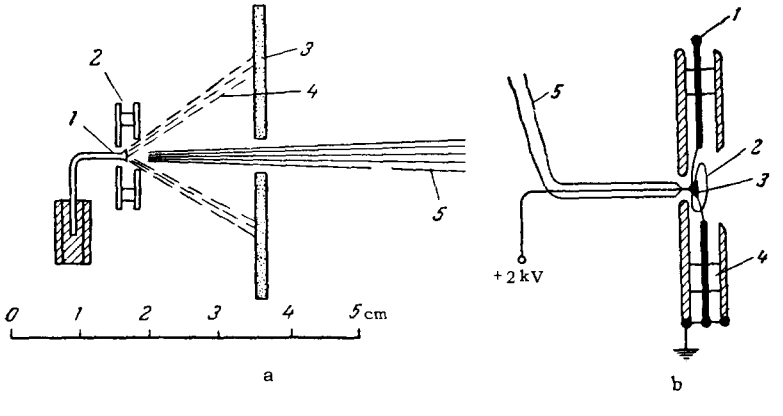

FIG. 47. a) Diagram showing sputtering by an ion beam of a target heated by electron bombardment: 1 – target, 2 – electron gun, 3 – collector, 4 – ejected atoms, 5 – ion beam; b) details of electron gun for heating the target: 1 – current lead, 2 – filament, 3 – target, 4 – glass insulator, 5 – thermocouple leads.

column of the diffraction apparatus, and also determination of the surface orientation of the specimens studied and the study of changes in their structure under bombardment, by the method of micro-diffraction. The specimen holder allowed heating the specimen up to 1500°C and inclining the specimen within the limits of 0 to 70°. From the specimen surfaces subjected to ion bombardment, carbon-platinum replicas were made which were scanned with an electron microscope with a resolution of 30 to 40 Å. Electron microscope photographs obtained from such replicas are shown in Fig. 25.

For sensitive measurement of the sputtering yield from bombardment of metallic single-crystal and polycrystalline films by low energy ions (30—200 eV), Medved and Poppa[120,121] used a Hitashi HU-10 electron microscope with an ion gun built into the object chamber (Fig. 48) and a Faraday cup in the plane of the diffraction image (operation in the micro-diffraction regime). Kr^+, Ar^+, and Ne^+ ions could be obtained from the ion gun. Monitoring of the sputtering was based on the variation of the scattering of the electron beam in the microscope with the thickness of the specimen. With this method it was possible to measure thickness changes of 4 Å for a film thickness of 100 Å. The limit of sensitivity to loss of mass depended on the cross section of the electron beam, and for a diameter of 2 μ was 2×10^{-14} g. Simultaneously with the measurement of the sputtering yield, it was possible to observe changes in the structure of the objects subjected to ion bombardment.

Considerably higher bombarding ion energies (up to 4 keV with an ion density of 2 $\mu A/mm^2$) have been obtained by Castaing and Jouffrey[122] using an ion gun mounted in an electron microscope close to the object stage. The axis of the ion beam was inclined

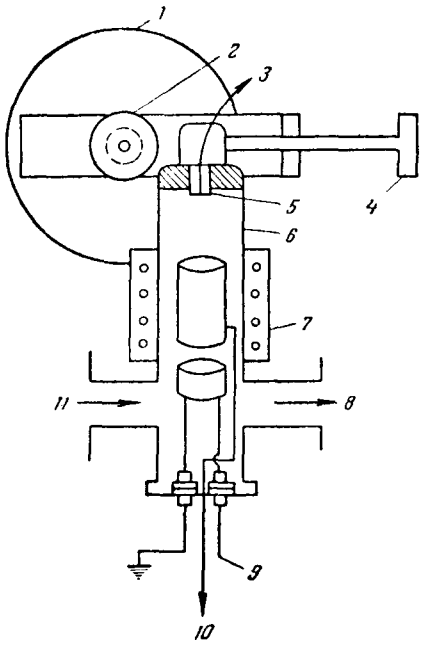

FIG. 48. Diagram showing the mounting of the ion gun in the column of the electron microscope. 1 – Electron-microscope column; 2 – location of sample chamber in the observation position; 3 – direction of rotation of specimens; 4 – extracting and rotating mechanism for moving the specimen from the sputtering position to the observation position; 5 – specimen; 6 – discharge region; 7 – magnets; 8 – to pump; 9 – control and heat shield leads; 10 – positive voltage; 11 – gas inlet.

at an angle of 30° to the axis of the electron microscope. This design permitted observation of the changes occurring in single-crystal gold foils during the ion bombardment process. The characteristic line distortions obtained in bombardment and the completely darkened phase contrast pictures were completely eliminated by subsequent annealing.

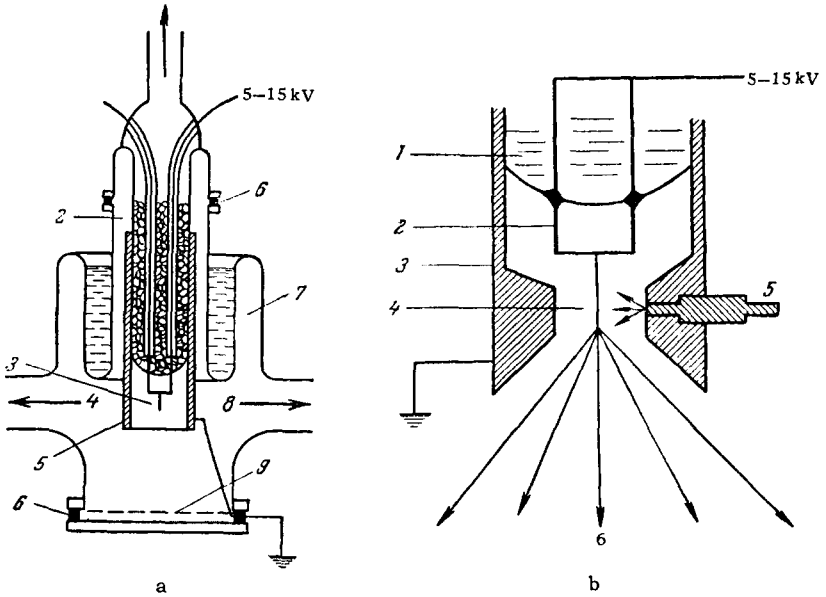

FIG. 49. a) Diagram of ion projection tube: 1 – centrifugal pump, 2 – dry nitrogen, 3 – specimen, 4 – to vacuum pumps, 5 – copper cylinder, 6 – indium gasket, 7 – liquid nitrogen, 8 – collector, to helium tank, 9 – fluorescent screen. b) Diagram of apparatus for bombarding a specimen by α particles in the course of observation in the projection tube: 1 – liquid nitrogen, 2 – tungsten stems, 3 – copper cylinder, 4 – specimen, 5 – α source, 6 – helium ions moving from the point of the specimen to the screen.

11.4. Observation of Focusons With the Ion Projector

Figure 49a shows a diagram of an ion projector used by Brandon and Wald [123] to observe point defects produced in tungsten by irradiation. Their specimens, while under observation in a projection tube, were irradiated by α particles emitted from a polonium source located near the specimen. A diagram of the experimental arrangement is shown in Fig. 49b. On the average one α particle hit the point of the specimen every three hours.

11.5. The Preparation of Thin Single-crystal and Polycrystalline Metallic Targets

For the preparation of thin single-crystal films (from 100 Å to 1—3μ), the usual technique widely used in electron microscopy [124] is the vacuum evaporation of the metal onto the surfaces of heated ionic crystals with the desired orientation. [45,125]

Polycrystalline foils are prepared by rolling and subsequent annealing, which leads to a definite preferred orientation of up to 90% of the crystallites, [47] or by chemical thinning. [121] Since contamination of the target surfaces has an important effect on the results of sputtering studies, the specimens are usually cleaned by ion bombardment before the experiment.

[1] F. Seitz and J. S. Koehler, Solid State Physics, F. Seitz and D. Turnbull ed., vol. 2, N. Y., 1956, page 307.

[2] G. H. Kinchin and R. S. Pease, Repts. Prog. Phys. 18, 1 (1955); Russ. trans., UFN 60, 590 (1956).

[3] C. Lehman, Nukleonik (Germany) 3, 1 (1961).

[4] G. J. Dienes and G. H. Vineyard, Radiation Effects in Solids, New York, Interscience, 1957. Russ. trans., IL, Moscow, 1960.

[5] Lifshitz, Kaganov, and Tanatarov, Atomnaya énergiya (Atomic Energy) No. 6, 391 (1959).

[6] J. A. Brinkman, J. Appl. Phys. 25, 961 (1954).

[7] J. A. Brinkman, Amer. J. Phys. 24, 246 (1956).

[8] G. K. Wehner, J. Appl. Phys. 25, 270 (1954).

[9] R. H. Silsbee, J. Appl. Phys. 28, 1246 (1957).

[10] G. Leibfried, J. Appl. Phys. 30, 1388 (1959).

[11] G. Leibfried, J. Appl. Phys. 31, 117 (1960).

[12] C. Lehman and G. Leibfried, Z. Physik 162, 203 (1961).

[13] P. H. Dederichs and G. Leibfried, Z. Physik 170, 320 (1962).

[14] E. M. Baroody, Phys. Rev. 124, 745 (1961).

[15] R. Frere, in Radiation Damage in Solids (Symposium, Venice, May 7—11, 1962), vol. 1, Vienna, 1962, page 87.

[16] Gibson, Goland, Milgram, and Vineyard, Phys. Rev. 120, 1229 (1960).

[17] D. E. Harrison, J. Appl. Phys. 32, 924 (1961).

[18] D. McKeown, Rev. Sci. Instr. 32, 133 (1961).

[19] Ionnye plazmennye i dugovye raketnye dvigateli (Ionic Plasma and Arc Rocket Engines), Gosatomizdat 1961, page 73.

[20] R. S. Pease, Rend. Scuola internaz. fis. E. Fermi 13, 158 (1960).

[21] L. A. Artsimovich, Upravlyaemye termoyadernye reaktsii (Controlled thermonuclear reactions) Fizmatgiz, Moscow, 1961.

[22] F. Seitz, Disc. Farad. Soc., No. 5, 271 (1949).

[23] E. C. H. Silk and R. S. Barnes, Phil. Mag. 4, 970 (1959).

[24] R. S. Barnes and D. J. Mazey, Phil. Mag. 5, 1247 (1960).

[25] Barnes, Redding, and Cottrell, Phil. Mag. 3, 97 (1958).

[26] R. S. Barnes, Disc. Farad. Soc., No. 31, 38 (1961).

[27] D. W. Pashley and A. E. B. Presland, Phil. Mag. 6, 1003 (1961).

[28] F. Seitz, Phys. Today 5, No. 6, (1952).

[29] A. M. Kosevich and L. V. Tanatarov, FTT 2, 3012 (1960). Soviet Phys. Solid State 2, 2676 (1961).

[30] U. Gonser and B. Okkerse, Phys. Rev. 105, 757 (1957).

[31] F. E. Fujita and U. Gonser, J. Phys. Soc. Japan 13, 1068 (1958).

[32] U. Gonser and B. Okkerse, J. Phys. Chem Solids 7, 55 (1958).

[33] Westmacott, Roberts, and Barnes, AERE-R 4096, 1 (1962); See Phil. Mag. 7, 2035 (1962).

[34] Makin, Whapham, and Minter, Phil. Mag. 7, 285 (1962).

[35] S. T. Konobeevskiĭ, Atomnaya énergiya (Atomic Energy), No. 2, 63 (1956).

[36] G. H. Kinchin and R. S. Pease, J. Nucl. Energy 1, 200 (1955).

[37] L. R. Aronin, J. Appl. Phys. 25, 344 (1954).

[38] H. B. Huntington, Phys. Rev. 91, 1092 (1953).

[39] H. Paneth, Phys. Rev. 80, 708 (1950).

[40] W. M. Lomer and A. H. Cottrell, Phil. Mag. 46, 711 (1955).

[41] A. Seeger, Proc. 2nd UN Int. Conf. Peaceful Uses of Atomic Energy 6, 250 (1958).

[42] A. Seeger, in Radiation Damage in Solids (Symposium, Venice, May 7—11, 1962), vol. 1, Vienna, 1962, page 10.

[43] A. H. Cottrell, Metallurg. Rev. 1, 479 (1956).

[44] V. E. Yurasova and I. G. Sirotenko, JETP 41, 1359 (1961). Soviet Phys. JETP 14, 968 (1962).

[45] R. S. Nelson and M. W. Thompson, Proc. Roy. Soc. A259, 458 (1961).

[46] J. A. Brinkman, in Radiation Damage in Solids, Intern. Summer School Lectures at Ispra, 1960.

[47] R. S. Nelson and B. W. Farmery, AERE-R 4192, 1 (1962).

[48] M. Balarin, Phys. Status Solidi 2, 60 (1962).

[49] G. K. Wehner, J. Appl. Phys. 25, 270 (1954).

[50] G. K. Wehner, J. Appl. Phys. 26, 1056 (1955).

[51] G. K. Wehner, Phys. Rev. 102, 690 (1956).

[52] E. Langberg, Phys. Rev. 111, 91 (1958).

[53] V. E. Yurasova, ZhTF 28, 1966 (1958). Soviet Phys. Technical Phys. 3, 1806 (1959).
[54] Yurasova, Spivak, and Kushnir, Izv. AN SSSR, ser. Fiz. 23, 744 (1959). Columbia Tech. Transl. p. 739.
[55] M. Koedam and A. Hoogendoorn, Physica 26, 351 (1960).
[56] Yurasova, Pleshivtsev, and Orfanov, JETP 37, 966 (1959). Soviet Phys. JETP 10, 689 (1960).
[57] M. Koedam, Phillips Res. Rep. 16, 101, 226 (1961).
[58] G. K. Wehner, Appl. Sci. Res. (Hague) B5, 334 (1957); Proc. 3rd Int. Conf. Ioniz. Phen. Gases, Venice, 1957, p. 1125.
[59] M. Koedam, Proc. 4th Int. Conf. Ioniz. Phen. Gases, Uppsala, 1954, p. 252.
[60] B. Dj. Perovic, Bull. Boris Kidrich Inst. Nucl. Sci. 11, 37 (1961).
[61] R. S. Nelson and M. W. Thompson, Phil. Mag. 7, 1425 (1962).
[62] P. Haymann and K. Mihama, Proc. Europ. Reg. Conf. Electron Microscopy (Delft, 1960), vol. 1, Delft, S. A., p. 253.
[63] P. Haymann, Metaux (Corrosion industries) 37, No. 441—444 (1962).
[64] Rol. Fluit, and Kisteraker, Proc. 3rd Int. Conf. Ioniz. Phen. Gases, Venice, 1957, p. 871.
[65] M. Koedam, Physica 25, 742 (1959).
[66] O'Briain, Lindner, and Moore, J. Chem. Phys. 29, 3 (1958).
[67] B. Cobić and B. Perović, Proc. 4th Int. Conf. Ioniz. Phen. Gases, Uppsala, 1959, p. 260.
[68] G. K. Wehner and D. Rosenberg, J. Appl. Phys. 31, 177 (1960).
[69] M. W. Thompson, Nucleonics, No. 6, 133 (June, 1960).
[70] L. A. Girifalco and J. R. Streetman, J. Phys. Chem. Solids 4, 182 (1958).
[71] L. A. Girifalco and V. G. Weizer, J. Phys. Chem. Solids 12, 260 (1960).
[72] R. S. Nelson and M. W. Thompson, Phys. Letters 2, 124 (1962).
[73] G. S. Anderson and G. K. Wehner, J. Appl. Phys. 31, 2305 (1960).
[74] G. S. Anderson, J. Appl. Phys. 33, 2017 (1962).
[75] V. E. Yurasova and E. A. Murinson, Izv. AN SSSR, ser. Fiz. 26, 1445 (1962), Columbia Tech. Transl. p. 1470.
[76] N. Bohr, The Penetration of Atomic Particles through Matter, Copenhagen, 1948; Russ. trans., IL, Moscow, 1950.
[77] Nelson, Thompson, and Montgomery, Phil. Mag. 7, 1385 (1962).
[78] V. E. Yurasova and V. M. Bukhanov, Kristallografiya 7, No. 2, 257 (1962), Soviet Phys. Crystallography 7, 199 (1962).
[79] Molchanov, Tel'kovskiĭ, and Shakh-Melikova, ZhTF 32, 647 (1962). Soviet Phys. Technical Physics 7, 469 (1962).
[80] Balarin, Molchanov, and Tel'kovskiĭ, DAN SSSR 147, 331 (1962). Soviet Phys. Doklady 7, 100 (1963).
[81] V. A. Molchanov and V. G. Tel'kovskiĭ, DAN SSSR 136, 801 (1961). Soviet Phys. Doklady 6, 137 (1961).
[82] Dushikov, Molchanov, Tel'kovskiĭ, and Chicherov, ZhTF 31, 1012 (1961). Soviet Phys. Technical Phys. 6, 735 (1962).
[83] V. A. Molchanov and V. G. Tel'kovskiĭ, Izv. AN SSSR, ser. Fiz. 26, 1359 (1962). Columbia Tech. Transl. p. 1381.
[84] Molchanov, Soshka, and Faruk, ZhTF 33, 766 (1963). Soviet Phys. Technical Physics 8, 573 (1963).
[85] Molchanov, Tel'kovskiĭ, and Chicherov, DAN SSSR 137, 58 (1961). Soviet Phys. Doklady 6, 222 (1961).
[86] Molchanov, Tel'kovskiĭ, and Chicherov, DAN SSSR 138, 824 (1961). Soviet Phys. Doklady 6, 486 (1961).
[87] E. S. Mashkova and V. A. Molchanov, DAN SSSR 146, 585 (1962). Soviet Phys. Doklady 7, 829 (1963).
[88] D. G. Brandon and P. B. Bowden, Phil. Mag. 6, 707 (1961).
[89] D. G. Brandon and P. B. Bowden, Disc. Farad. Soc., No. 31, 70 (1961).
[90] Ruedl, Delavignette, and Amelinckx, Phys. Rev. Letters 6, 530 (1961).
[91] Ruedl, Delavignette, and Amelinckx, Disc. Farad. Soc., No. 31, 69 (1961).
[92] Ruedl, Delavignette, and Amelinckx, in Radiation Damage in Solids (Symposium, Vienna, May 7—11, 1962), vol. 1, Vienna, 1962, p. 363.
[93] E. W. Müller, UFN 77, 481 (1962). A translation of Adv. in Electronics and Electron Physics 13, 83 (1960).
[94] D. G. Brandon and M. Wald, Disc. Farad. Soc. No. 31, 73 (1961).
[95] A. Sosin, in Radiation Damage in Solids (Symposium, Venice, May 7—11, 1962), vol. 1, Vienna, 1962, p. 223.
[96] M. J. Makin and T. H. Blewitt, Acta Met. 10, 241 (1962).
[97] Thompson, Blewitt, and Holmes, J. Applied Phys. 28, 742 (1957).
[98] D. S. Billington, Nucleonics 14, No. 9, 54 (Sept. 1956).
[99] M. W. Thompson, in Radiation Damage in Solids (Symposium, Venice, May 7—11, 1962), vol. 1, Vienna, 1962, p. 239.
[100] O. A. Troitskiĭ and V. I. Likhtman, DAN SSSR 148, 332 (1963). Soviet Phys. Doklady 8, 91 (1963).
[101] E. N. da C. Andrade, Nature (London) 156, 113 (1945).
[102] R. I. Garber and I. A. Gindin, UFN 74, 31 (1961). Soviet Phys. Uspekhi 4, 405 (1961).
[103] M. J. Makin, J. Nucl. Energy 1, 181 (1955).
[104] F. Seitz, Science 138, 563 (1962).
[105] Dauntreppe, Langier, Paulevé, and Néel, in Radiation Damage in Solids (Symposium, Venice, May 7—11, 1962), vol. 2, Vienna, 1962, p. 21.

[106] U. Gonser, J. Nucl. Mater. 2, 43 (1960).
[107] N. A. Kaptsov, Élektricheskie yavleniya v gazakh i vakuume (Electrical Phenomena in Gases and Vacuum), Gostekhizdat, Moscow, 1950.
[108] A. von Engel and M. Steenbeck, Elektrische Gasentladungen, ihre Physik und Technik, Edwards Bros., Ann Arbor, 1944.
[109] L. B. Loeb, Fundamental Processes of Electrical Discharges in Gases, Wiley, N. Y., 1939.
[110] G. K. Wehner, Adv. in Electronics and Electron Phys., vol. 7, N. Y., 1955, page 260.
[111] P. Wolsky and E. J. Zdanuk, Vacuum 10, 13 (1960).
[112] N. Laegreid and G. K. Wehner, J. Appl. Phys. 32, 365 (1961).
[113] L. N. Dobretsov and N. M. Karnaukhova, DAN SSSR 85, 745 (1952).
[114] M. A. Eremeev and Ya. K. Éstrinov, ZhTF 22, 1552 (1952).
[115] M. I. Guseva, PTÉ, No. 5, 112 (1957).
[116] M. von Ardenne, Technik 2, 65 (1958).
[117] I. V. Orfanov and V. A. Teplyakov, PTÉ, No. 2, 150 (1960).
[118] R. C. Bradley and E. Rudel, J. Appl. Phys. 33, 880 (1962).
[119] Barnfield, Farmery, Hobbis, Nelson, and Thompson, J. Nucl. Energy C4, 2 (1962).
[120] D. B. Medved and H. Poppa, J. Appl. Phys. 33, 1759 (1962).
[121] H. Poppa, Phil. Mag. 7, 1013 (1962).
[122] R. Castaing and B. Jouffrey, Colloq. Intern. Centre nat. rech. scient., No. 113, 63 (1962).
[123] A. H. Cottrell, J. Inst. Metals 90, 449 (1962).
[124] "Novye élektronnomikroskopicheskie issledovaniya" (New Electron-microscopic Studies), at Metallurgizdat, 1961.
[125] V. A. Phillips, Phil. Mag. 5, 571 (1960).
[126] M. Yoshida, J. Phys. Soc. Japan 16, 44 (1961).

Translated by C. S. Robinson